

ANALYSIS OF THE ROLE OF TALIN AS A MECHANOSENSOR AT THE CELL  
ADHESIONS TO THE EXTRACELLULAR MATRIX IN *DROSOPHILA MELANOGASTER*

by

GUDLAUG KATRIN HAKONARDOTTIR

B.Sc., University of Iceland, 2011

A THESIS SUBMITTED IN PARTIAL FULFILLMENT OF  
THE REQUIREMENTS FOR THE DEGREE OF  
MASTER OF SCIENCE

in

THE FACULTY OF GRADUATE AND POSTDOCTORAL STUDIES

(Cell and Developmental Biology)

THE UNIVERSITY OF BRITISH COLUMBIA

(Vancouver)

April 2015

© Gudlaug Katrin Hakonardottir, 2015

## Abstract

Cells in multicellular organisms are arranged in complex three-dimensional patterns. To achieve such complexity, cells must form adhesive contacts with the extracellular matrix (ECM). The most common adhesion receptors that mediate cell-ECM adhesions are the integrins. A large cytoplasmic network of proteins, namely the integrin adhesion complex (IAC) is recruited to the site of adhesions. Regulated assembly and disassembly, or turnover, of the IAC is essential for dynamic cell movements and tissue maintenance. In this project, I sought to investigate the role of mechanical force on the turnover of talin, a core component of the IAC and an essential linker between integrins and the actin cytoskeleton.

To investigate the turnover of talin *in vivo*, I performed fluorescence recovery after photobleaching (FRAP) on the myotendinous junctions (MTJs) in live *Drosophila* embryos and larvae. I used temperature sensitive mutants to alter the force acting on the MTJs. To better understand talin turnover, I collaborated with people from Dan Coombs' lab (Department of Mathematics, UBC) to develop a mathematical model for the turnover of cytoplasmic adhesion proteins. This model is parametrized by four rate constants: talin binding on and off the adhesion complex at the plasma membrane, talin delivery to the plasma membrane due to the assembly of the IAC and talin removal from the plasma membrane due to the disassembly of the IAC.

I hypothesized that changes in force would affect talin turnover and certain functional domains in talin would be required for mechanosensing at the MTJs. I used targeted point mutations in the functional domains of talin to investigate their role in mechanosensing. Consistent with my hypothesis, I found out that disrupting functional domains in talin either abrogates or severely

affect the ability of talin to respond to changes in force. First, these results provide direct evidence on how force is sensed at the adhesion complex. Secondly, this is the first *in vivo* study where four rate constants are used to characterize the turnover of a cytoplasmic protein.

## **Preface**

Dr. Guy Tanentzapf and I designed the work presented in this thesis. I performed all the fly genetics, collected, analyzed, and interpreted FRAP data, and produced all the figures with the exception of Figure 8. Alejandra Herrera developed and performed the mathematical analysis to derive the rate constants. Pablo Lopez performed the drug delivery experiments. Michael J. Fairchild produced the talin mutant constructs. Walter Wasserman and Katie Goodwin calculated the mobile fractions.

## Table of Contents

<b>Abstract</b> .....	<b>ii</b>
<b>Preface</b> .....	<b>iv</b>
<b>Table of Contents</b> .....	<b>v</b>
<b>List of Tables</b> .....	<b>viii</b>
<b>List of Figures</b> .....	<b>ix</b>
<b>List of Abbreviations</b> .....	<b>x</b>
<b>Acknowledgements</b> .....	<b>xii</b>
<b>Dedication</b> .....	<b>xiii</b>
<b>Chapter 1: INTRODUCTION</b> .....	<b>1</b>
1.1 Integrins and the IAC (integrin adhesion complex).....	1
1.1.1 Integrins - domain structure and binding partners .....	1
1.1.2 The IAC .....	3
1.1.3 Importance of integrin mediated adhesions – brief overview.....	5
1.1.4 Integrins as mechanosensors.....	6
1.2 Talin – structure and function.....	7
1.2.1 Talin – domain structure and binding partners .....	7
1.2.2 Talin mediated integrin activation .....	9
1.2.3 Talin autoinhibition.....	10
1.2.4 Talin and vinculin as mechanotransducers .....	11
1.2.5 Talin mediated linkage to the cytoskeleton .....	12
1.3 Integrin mediated adhesions in <i>Drosophila</i> .....	13
1.3.1 Integrins in <i>Drosophila</i> .....	13
1.3.2 Talin in <i>Drosophila</i> .....	14
1.3.3 The IAC in <i>Drosophila</i> .....	14
1.3.4 Structure-function analysis of talin.....	15

1.3.5	The MTJs in <i>Drosophila</i> as a model to study cell-ECM adhesions .....	16
1.4	Turnover of integrins and the IAC components .....	17
1.4.1	Studies in cell culture.....	18
1.4.2	Role of the endocytic machinery in turnover.....	19
1.4.3	Studies in <i>Drosophila</i> .....	21
1.4.4	Regulation of talin turnover by force.....	23
1.4.5	Rate constants to describe the turnover of the adhesion proteins .....	24
1.5	Objectives, rationale and hypotheses.....	26
1.5.1	Objective.....	26
1.5.2	Hypothesis.....	26
1.5.3	Rationale .....	26
<b>Chapter 2: MATERIALS AND METHODS.....</b>		<b>28</b>
2.1	Fly stocks and lines.....	28
2.2	FRAP experiments .....	29
2.2.1	Live imaging – whole mount sample preparation.....	29
2.2.2	Confocal microscope settings for FRAP experiments .....	29
2.2.3	Temperature sensitive sample preparation.....	30
2.2.4	Inhibition of endocytosis in live embryos.....	30
2.3	Mathematical analysis of FRAP data.....	30
2.3.1	Cytoplasmic model .....	31
2.3.2	Double fitting to derive rate constants .....	32
2.3.3	Mobile fraction analysis.....	34
<b>Chapter 3: RESULTS.....</b>		<b>35</b>
3.1	Developing a model for the turnover of cytoplasmic proteins .....	35
3.2	Analysis of talin turnover in response to altered force .....	37
3.2.1	Talin turnover in response to increased force .....	38
3.2.2	Talin turnover in response to decreased force .....	44
3.3	Talin turnover in development.....	51

<b>Chapter 4: DISCUSSION AND CONCLUSIONS.....</b>	<b>53</b>
4.1 Model for cytoplasmic proteins to gain mechanistic insight into turnover .....	53
4.2 Analysis of talin turnover in response to increased force .....	55
4.2.1 Increased $K_{asm}$ is the main method of turnover regulation in response to increased force in WT talin.....	55
4.2.2 $K_{asm}$ becomes dysregulated in all of the talin mutants in response to increased force .....	56
4.2.3 $K_{on}$ becomes more dominant than $k_{off}$ in response to increased force for WT and talin mutants.....	57
4.2.4 $K_{on}$ and $k_{off}$ become dysregulated in the actin binding mutant in response to increased force .....	57
4.3 Analysis of talin turnover in response to decreased force .....	58
4.3.1 Decreased force does not affect the mobile fraction of WT talin.....	58
4.3.2 Decreased force causes dysregulation in the turnover of talin that contains the IBS-2 mutant.....	59
4.3.3 Decreased force does not severely affect the turnover of WT talin, activation-, IBS-1-, and actin binding mutants .....	60
4.4 Proposed model of integrin and talin turnover .....	61
4.5 During <i>Drosophila</i> embryogenesis and larval development there are two mechanisms that regulate talin turnover.....	65
4.6 Conclusions.....	66
<b>Bibliography .....</b>	<b>68</b>
<b>Appendices.....</b>	<b>74</b>
Appendix A - Mathematical analysis of FRAP data (author: Alejandra Herrera, 2015) ....	74
Appendix B - Dynasore datasets used for „double fitting“. .....	78
Appendix C - Tables with mobile fraction and rate constant values.....	79

## List of Tables

Table 1: Talin mutations used in this study. ....	16
---	----

## List of Figures

Figure 1: Schematics of Integrins. ....	3
Figure 2: Schematic of integrins, the IAC and the cytoskeleton (shown as F-actin).....	5
Figure 3: Schematic of talin domain structure and binding sites. ....	9
Figure 4: Schematic of the localization of the talin mutants used in this study.....	16
Figure 5: Schematic of the MTJs, the muscle-tendon attachments sites in <i>Drosophila</i> . ....	17
Figure 6: FRAP (fluorescence recovery after photobleaching). ....	24
Figure 7: Schematics of the cytoplasmic model for talin. ....	25
Figure 8: Development of the mathematical model to characterize turnover for cytoplasmic proteins.....	35
Figure 9: Turnover of WT talin in Brkd <sup>J29</sup> background.....	39
Figure 10: Turnover of talin mutants in Brkd <sup>J29</sup> background. ....	42
Figure 11: Turnover of WT talin in para <sup>ts2</sup> background. ....	45
Figure 12: Turnover of talin mutants in para <sup>ts2</sup> background. ....	48
Figure 13: Turnover of WT talin in development (heterozygous background).....	51
Figure 14: Proposed model of turnover for WT integrin and talin in response to altered force...	63
Figure 15: Dynasore experiments used for double fitting. ....	78

## List of Abbreviations

ABS	actin binding site
AFM	atomic force microscopy
CCSs	clathrin-coated structures
CHO	chinese hamster ovary
DC	dorsal closure
DD	dimerization domain
e17	embryonic stage 17
ECM	extracellular matrix
EEs	early endosomes
FA	focal adhesions
FAK	focal adhesion kinase
FERM	protein 4.1, ezrin, radixin, moesin
FRAP	fluorescence recovery after photobleaching
GFP	green fluorescent protein
HIP1	Huntingtin-interacting protein
IAC	integrin adhesion complex
IBS1	integrin binding site 1
IBS2	integrin binding site 2
l3	third larval stage / third instar
LDV	leucine-aspartate-valine
MOP	membrane orientation patch
MTJs	myotendinous junctions
NMR	nuclear magnetic resonance
ODE	ordinary differential equations
PBS	phosphate buffered saline
PIP1 $\gamma$ 90	phosphatidylinositol-4-phosphate 5-kinase type 1 $\gamma$ 90
PNCr	perinuclear recycling compartment
PS	position specific
PTB	phosphotyrosine binding
RGD	arginine-glycine-aspartate
RIAM	Rap1-GTP-interacting adaptor molecule
scab	Scabrous

SMD	steered molecular dynamics
SEM	standard error of the mean
siRNA	short interfering RNA
THATCH	talin/HIP1R/Sla2p Actin-Tethering C-terminal Homology
TIRFM	total internal reflection microscopy
VBS	vinculin binding site
WT	wild type

## **Acknowledgements**

First, I would like to thank my supervisor Guy Tanenzapf for giving me the opportunity to join his lab to pursue my degree. He constantly gave me constructive criticisms throughout my time in his lab.

Secondly, I would like to thank the two people who collaborated with me on this project. Without Alejandra Herrera and Pablo Lopez the thesis presented herein would not exist. I would also like to thank past and present members of the Tanenzapf lab. In particular, Stephanie Ellis, Fayeza Islam, Michael Fairchild, Alex Morin, Alexander Perkins, Chris Smendziuk, Katie Goodwin, Emily Lostchuck and Daniella Gunne. Working with you throughout the past two and a half year has truly been a great experience.

Thirdly, I would like to thank my committee members Shernaz Bamji and Dan Coombs, and my examining committee Doug Altshuler and John Church for their time.

Finally, I would like to thank my husband, Dadi Baldur Ottosson, and my parents and friends for their support. I love you all.

## **Dedication**

I dedicate this thesis to my mom and dad.

# Chapter 1: INTRODUCTION

## 1.1 Integrins and the IAC (integrin adhesion complex)

### 1.1.1 Integrins - domain structure and binding partners

Integrins are the major protein family that mediates adhesions between cells and the ECM (Hynes, 1987). Integrins are transmembrane heterodimeric receptors that are made up of an  $\alpha$  and a  $\beta$  subunit. Integrins are conserved in all metazoans but the number of the  $\alpha$  and  $\beta$  isoforms varies between species. Each heterodimer is a single pass transmembrane protein that has a large extracellular domain, small transmembrane domain and a short cytoplasmic tail composed of 20-70 amino acids (Figure 1). To date, 18  $\alpha$  and 8  $\beta$  subunits that can dimerize in 24 known  $\alpha\beta$  combinations have been found in the mammalian genome (reviewed in Humphries et al. (2006)). Integrin heterodimers can have a tissue specific expression pattern. For example, in *Drosophila melanogaster*  $\alpha$ PS2 $\beta$ PS binds to specialized ECM (extracellular matrix) that is found at the muscle attachment sites (Prokop et al., 1998).

Integrins mediate cell adhesions to the ECM by binding directly to different ECM ligands. Different integrin heterodimers have varying affinity for different ECM ligands. In addition, some ECM ligands bind to multiple integrin heterodimers. It is possible to classify integrin-ECM ligand pairs into four groups based on the structural basis of the molecular interaction. These classes are: RGD<sup>1</sup> binding integrins, LDV<sup>2</sup> binding integrins, A-domain  $\beta$ 1 integrins and

---

<sup>1</sup> arginine-glycine-aspartate

<sup>2</sup> leucine-aspartate-valine

non- $\alpha$ A-domain-containing laminin binding integrins. Fibronectin, vitronectin and fibrinogen are examples of ECM ligands that contain the RGD motif. Other ECM ligands that integrins bind to include laminin and collagen (reviewed in Humphries et al. (2006)). Binding of ECM ligands to integrins causes a conformational change in the entire molecule that results in increased affinity of the integrin cytoplasmic tail for cytoplasmic ligands (reviewed in (Askari et al., 2009)).

On the inside of the cell, the short cytoplasmic tail of integrins interacts with relatively few proteins. Some of these include the signaling proteins ILK and FAK (reviewed in Liu et al. (2000)). The most notable is the integrin-activator and actin binding protein talin that links integrins to the cytoskeleton (see 1.2 for detailed discussion) (Horwitz et al., 1986; McCann and Craig, 1999). Furthermore, it has been shown that kindlin 1 and kindlin 2 interact with the  $\beta$  integrin cytoplasmic tail to co-activate integrins (Harburger et al., 2009).

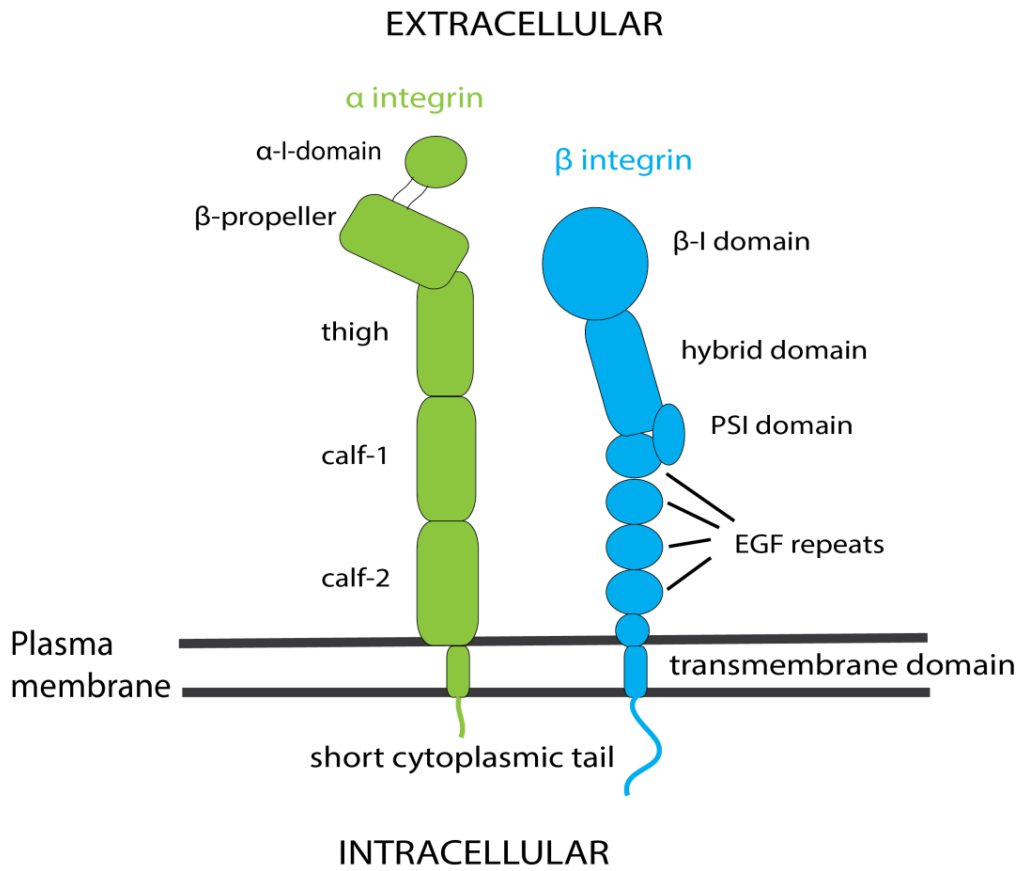


**Figure 1: Schematics of Integrins.**

Integrins have a large extracellular domain, small transmembrane domain and a short cytoplasmic tail. The major conserved domains are shown.

### 1.1.2 The IAC

The  $\beta$  integrin cytoplasmic tail recruits and assembles the integrin adhesion complex (IAC). The IAC is a network of interacting proteins that links integrins to the cytoskeleton (Figure 2). Talin is thought to be the only sole core component of the IAC as its absence mimics the phenotype caused by the loss of integrins in *Drosophila melanogaster* embryos. Furthermore, talin is the only IAC component that is absolutely required for integrin mediated adhesions (reviewed in (Brown et al., 2002; Bulgakova et al., 2012)).

The IAC includes integrin binding proteins, scaffolding proteins, actin-binding proteins and cell signalling proteins. To date, about 180 components have been found to be a part of the IAC. On average each component forms roughly eight interactions which results in a very dense protein network (reviewed in (Wolfenson et al., 2013; Zaidel-Bar and Geiger, 2010)).

The composition of the IAC depends on factors like ECM stiffness, tensile force and adhesion maturation. For example, the formation of nascent adhesions requires Arp2/Arp3 mediated actin polymerization while their maturation to large focal adhesions (FA) depends on myosinII-mediated cell contractility. In each mechanism, different sets of proteins are enriched at the adhesions (reviewed in Schiller and Fassler (2013)). Furthermore, quantitative proteomics using the myosinII inhibitor blebbistatin have shown that myosinII activity alters the protein composition of the integrin mediated adhesions (Schiller and Fassler, 2013; Schiller et al., 2011).

Multiple IAC components have been shown to be mechanosensitive such as talin (del Rio et al., 2009), vinculin (Dumbauld et al., 2013), p130-Cas (Sawada et al., 2006) and zyxin (Yoshigi et al., 2005) (see 1.2.4). When mechnosensitive components of the IAC are exposed to force they can undergo conformational changes that lead to recruitment of other proteins or they become phosphorylated and consequently change the composition of the IAC (del Rio et al., 2009; Sawada et al., 2006).

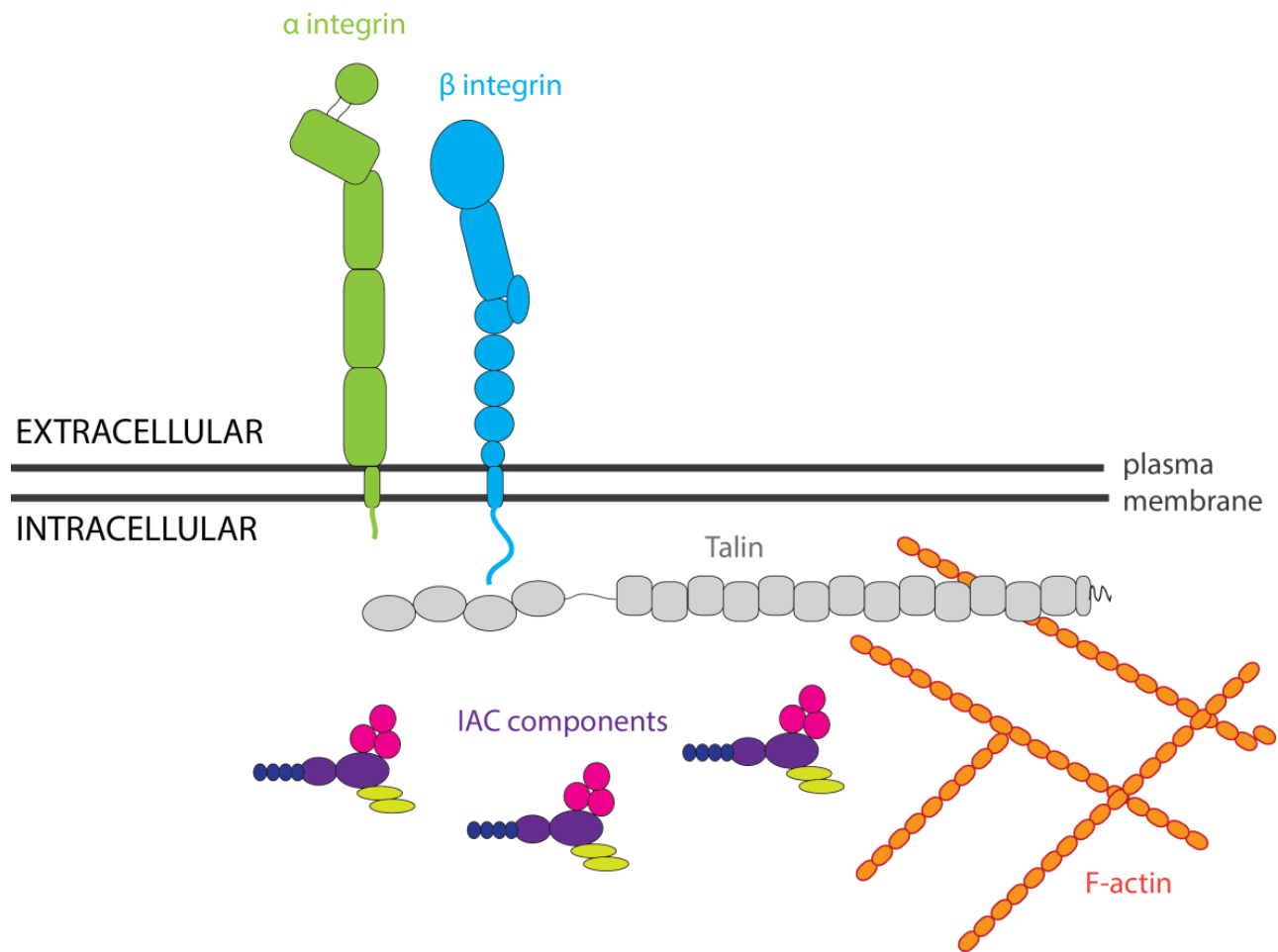


**Figure 2: Schematic of integrins, the IAC and the cytoskeleton (shown as F-actin).**

### 1.1.3 Importance of integrin mediated adhesions – brief overview

Integrin mediated cellular adhesions to the ECM play a crucial role in numerous processes in multicellular organisms including embryonic development, tissue formation, hemostasis, extracellular matrix assembly, and immune response. Integrins function in cell spreading and cell migration are central to afore mentioned processes (reviewed in (Brown et al., 2000; Hynes, 2002; Parsons et al., 2010). In *Drosophila*, integrins are known to play essential roles in

morphogenetic events such as germband retraction, dorsal closure and muscle attachments (reviewed in Brown et al. (2000)).

Furthermore, integrin function has been implicated in multiple diseases in humans. Thrombosis was the first disease-related process found to be related to integrin function. The formation of thrombus inside blood vessels requires  $\alpha\text{IIb}\beta\text{3}$  integrins (Ni and Freedman, 2003). Many integrin heterodimers have been implicated in various types of cancer (reviewed in Desgrosellier and Cheresh (2010). The integrin that has attracted most attention is the  $\alpha\text{V}\beta\text{3}$  because of its medical relevance. The  $\alpha\text{V}\beta\text{3}$  integrin has a key role in metastasis and has for example, been implicated in bone metastatic growth (Desgrosellier and Cheresh, 2010; McCabe et al., 2007).

#### **1.1.4 Integrins as mechanosensors**

Integrins are sensitive to force and it has been proposed that they can transduce force from one side of the plasma membrane to the other side which can initiate signalling events. The force can either be external (e.g. shear stresses or matrix stretching) or internal (e.g. driven by actomyosin contractility or actin polymerization) (reviewed in Geiger et al. (2009).

It has been shown that integrins can form catch bonds with their ECM ligands. The definition of catch bonds are receptor–ligand bonds that last longer when force is applied opposed to the ordinary slip bonds that last for a shorter period of time with the application of force (Kong et al., 2009). The increased bond lifetime allows multiple IAC components to be recruited to the adhesions sites to strengthen and enlarge the adhesions. This process is called “adhesion maturation”. The actin-myosin II network generates intracellular force and pulls on the integrin–ECM ligand bonds. Blocking the actomyosin II activity reduces the number of  $\alpha\text{5}\beta\text{1}$ –fibronectin

catch bonds. Furthermore, integrins can sense the stiffness of the ECM and strengthen the adhesions accordingly. The same research group has shown that cells plated on a stiff fibronectin coated substrate showed increased number of  $\alpha5\beta1$ -fibronectin catch bonds compared to cells plated on a softer substrate (Friedland et al., 2009).

Another aspect of integrins that has been proposed to be force-sensitive is the transition of the  $\beta$ -integrin inactive conformation to an active conformation. It was found out using steered molecular dynamics (SMD) that force accelerated a hinge-angle opening between the  $\beta$ -I-domain and the hybrid domain (see Figure 1 for schematic of integrin domains). This hinge-angle opening has been linked with integrin activation (Puklin-Faucher et al., 2006)

## **1.2 Talin – structure and function**

In this thesis, the main focus is on talin, a core component of the IAC. Therefore, the structure and functions of talin will be described in the sections below.

### **1.2.1 Talin – domain structure and binding partners**

Talin was first discovered in the 1980s by Keith Burridge (Burridge and Connell, 1983). Talin is composed of a globular N-terminal FERM (protein 4.1, ezrin, radixin, moesin) domain often referred to as the talin head and a flexible C-terminal rod that are separated by an unstructured linker region (Figure 3). The FERM domain is 50 kDa and is made up of four subdomains (F0, F1, F2 and F3) (Gingras et al., 2009). The rod is 200 kDa and is predicted to be made up of 62  $\alpha$ -helices that are organised into 13 amphipathic helical bundles (R1-R13) (Tempel et al., 1995).

In addition, *Drosophila* talin has an unstructured tail at the C-terminus (Figure 3) (Brown et al., 2002).

Talin contains multiple known protein interactions domains (Figure 3). For example, the talin head contains binding sites for the cytoplasmic domains of  $\beta$ -integrins (IBS-1) which is required for integrin activation (see 1.2.2), layilin (a hyaluronan receptor) and filamentous actin. The talin head also has binding sites for FAK and PIPK1 $\gamma$ 90 that regulate the dynamics of FA. A binding site for the small GTPase Rab1, a regulator of integrin-mediated cell adhesions is also located in the talin head (Bos, 2005).

The talin rod contains an additional integrin binding site (IBS-2) (see 1.2.1), at least two actin binding sites (ABS) and multiple vinculin binding sites (Figure 3) (Critchley and Gingras, 2008). The ABS near the far C-terminus contains a THATCH (or I/LWEQ) domain. THATCH is an actin binding module that can also be found in animal and amoebozoan talin, fungal Sla2 and its animal homologue Hip1. The THATCH domain contains a module that is responsible for talin dimerization that is required for its actin binding activity (Gingras et al., 2008; Smith and McCann, 2007). Finally, the R9 segment of the talin rod contains the autoinhibition domain responsible for forming an intramolecular bond with the FERM domain (see 1.2.3) (Goksoy et al., 2008).

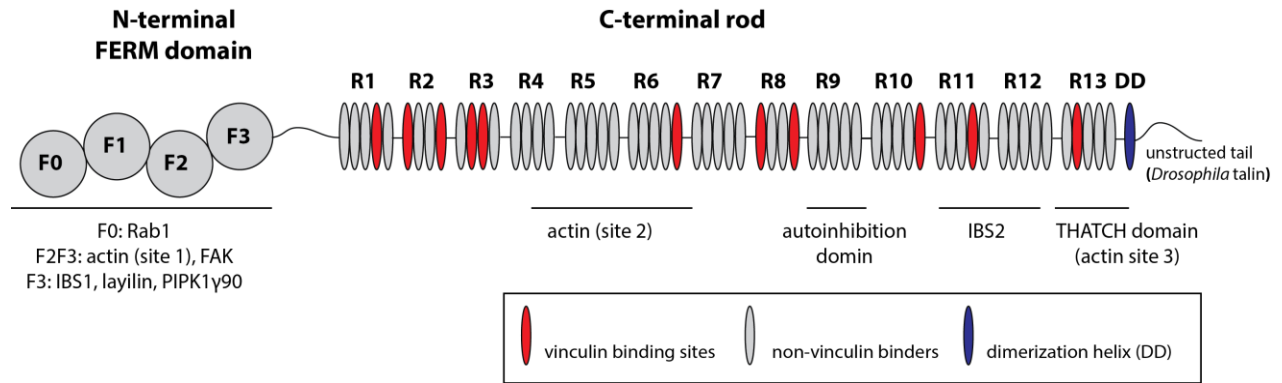


**Figure 3: Schematic of talin domain structure and binding sites.**

Modified from (Goult et al., 2013).

### 1.2.2 Talin mediated integrin activation

Conformational changes in the integrin heterodimer regulate its affinity for ECM ligands. Integrin heterodimers can adopt a series of conformational changes but in general, it is thought that they have three major conformational states. First, integrins can be ECM ligand occupied. Secondly, they can be active/primed (high affinity for ECM ligands). Lastly, they can be inactive (low affinity for ECM ligands) (Askari et al., 2009).

It has been demonstrated that binding of the talin head (namely the F3 subdomain) to the cytoplasmic tail of the  $\beta$ -integrin subunit promotes integrin activation (Calderwood et al., 1999). This process is often referred to as inside-out activation. In detail, a phosphotyrosine binding (PTB) domain in the talin F3 interacts with the membrane proximal NPxY<sup>3</sup> motif in the  $\beta$ -integrin cytoplasmic tail (Calderwood et al., 2002). In 2006, Iain D. Campbell and his research group sought to investigate talin's unique ability among PTB-containing proteins to activate

<sup>3</sup> Asparagine-Proline-X-Tyrosine. X donates any amino acid.

integrin by using NMR analysis. They elucidated an additional interaction between talin F3 and the membrane proximal (MP) region of the  $\beta$ -integrin cytoplasmic tail (Wegener et al., 2007). Binding of the talin head to the  $\beta$ -integrin cytoplasmic tail leads to disruption of salt bridges between the  $\alpha$  and the  $\beta$  integrin subunits that maintain the inactive state. Another feature which is required for talin mediated integrin activation is an interaction between a patch of positively charged lysine residues<sup>4</sup> in talin F2 and the negatively charged lipids in the plasma membrane. This interaction correctly orients talin to promote its interaction with the  $\beta$ -integrin cytoplasmic tail (Anthis et al., 2009).

Lastly, binding of the talin head to the  $\beta$ -integrin cytoplasmic tail causes separation of the  $\alpha$  and  $\beta$  transmembrane domains and leads to conformational changes in the entire integrin heterodimer that increases the affinity for ECM ligands (reviewed in (Hynes, 2002)). It is now evident that the binding of the talin head to the  $\beta$ -integrin cytoplasmic tail is sufficient to cause integrin activation in the absence of other proteins or external force (Ye et al., 2010).

### **1.2.3 Talin autoinhibition**

Talin regulates its own activity by autoinhibition, similar to other proteins with a FERM domain like moesin, FAK and kindlin (Tepass, 2009). The same region of the talin head that binds to the  $\beta$ -integrin cytoplasmic tail in integrin activation also binds to a region in the talin rod called the autoinhibition domain (Figure 3). Autoinhibition masks the integrin binding site (IBS-1) in the talin head resulting in inability to activate integrins (Goksoy et al., 2008). NMR studies by

---

<sup>4</sup> Alternatively called MOP – membrane orientaton patch

Benjamin T. Goult and Esen Goksoy have demonstrated that the talin rod competes with the  $\beta$ -integrin cytoplasmic tail for binding with the talin head (Goksoy et al., 2008; Goult et al., 2009). Additionally, it has been shown that mutations that relieve autoinhibition cause increased integrin activation (Goksoy et al., 2008).

Thus far, the relief of talin autoinhibition is not well understood but molecules like GTPase Rap1 and its binding partner RIAM (Rap1-GTP-interacting adaptor molecule) have been implicated in the process (Lee et al., 2009). In addition, the biological consequences of talin autoinhibition are not fully elucidated but studies in cell culture have shown that mutations that relieve autoinhibition cause increased rate of FA assembly (Kopp et al., 2010).

#### **1.2.4 Talin and vinculin as mechanotransducers**

Talin and its binding partner vinculin are mechanosensitive proteins (del Rio et al., 2009; Dumbauld et al., 2013; Galbraith et al., 2002). It has been shown that talin's ability to sense mechanical force can coordinate the maturation and the assembly of the adhesion complex via different processes.

Following is an example of how talin's binding partners are dependent on the force-induced conformational changes in the talin molecule. NMR studies have shown that vinculin binding sites overlap with RIAM binding sites in the N terminal region of the talin rod, thus vinculin and RIAM binding to talin are mutually exclusive. The same study also showed that RIAM and vinculin bind to talin by different modes. RIAM binds to unstretched talin rod but vinculin binding requires force-induced stretching of the rod (Goult et al., 2013). Furthermore, it has been shown by immunohistochemistry in murine fibroblasts that vinculin and RIAM exhibit

different localization within adhesions. RIAM strongly localizes at the membrane and in focal complexes in protrusions while vinculin is localized more centrally at the mature, force-bearing FA (Lee et al., 2013).

### **1.2.5 Talin mediated linkage to the cytoskeleton**

Talin links integrins to the cytoskeleton by directly binding actin or indirectly by recruiting other actin-binding proteins. Below I will discuss one example for each process. Direct linkage to the cytoskeleton can occur through talin's three known ABS (Smith and McCann, 2007) but the ABS at the far C-terminus that contains a THATCH domain (Figure 3) has been most studied. It has been shown that the THATCH domain is important for the first steps of integrin linkage to the cytoskeleton. Michael P. Sheetz and his colleagues used optical trap experiments to show that talin's THATCH domain is required for reinforcing 2 pN slip bond between ECM bound integrins and the cytoskeleton (Jiang et al., 2003).

One example of an indirect talin mediated linkage to the cytoskeleton is talin induced recruitment of vinculin and other adhesion components to the IAC (Ziegler et al., 2008). It has been shown that talin binds to vinculin via a force-dependant mechanism. Talin has multiple vinculin binding sites (VBS) (Figure 3) that are normally cryptic but experiments with magnetic tweezers, TIRFM and AFM have revealed that mechanical stretching of the talin rod exposes the VBS in a stretch level dependant manner (del Rio et al., 2009). Therefore, vinculin can bind to talin and crosslink it to actin (Yao et al., 2014). Finally, direct and indirect talin-mediated integrin linkages to the cytoskeleton that are outlined above are not mutually exclusive processes and can happen simultaneously.

### 1.3 Integrin mediated adhesions in *Drosophila*

In this study, I use *Drosophila melanogaster* to study integrin mediated adhesions. In general, *Drosophila* provides an excellent model system to study the function of adhesion proteins. First, *Drosophila* has much simpler and less redundant genome than vertebrates. Secondly, the *Drosophila* genome has orthologs for all the main components of the IAC. Finally, *Drosophila* embryo and larva are transparent making it possible to trace the components of the IAC in the context of an intact multicellular organism without additional treatment.

#### 1.3.1 Integrins in *Drosophila*

Integrins in *Drosophila* are named position specific (PS) because of their position specific expression pattern of  $\alpha$ PS1 and  $\alpha$ PS2 in mature wing discs (Brower et al., 1984). The *Drosophila* genome encodes five  $\alpha$  subunits:  $\alpha$ PS1 (*multiple edematous wings*),  $\alpha$ PS2 (*inflated*),  $\alpha$ PS3 (*scab/volado*),  $\alpha$ PS4,  $\alpha$ PS5 and two  $\beta$  subunits  $\beta$ PS (*mysospheroid*) and  $\beta$ PSV compared to eighteen  $\alpha$  subunits and eight  $\beta$  subunits that are encoded in vertebrates (reviewed in Brown et al. (2000)). The  $\beta$ PS subunit, encoded by the *mysospheroid* (*mys*) locus is the predominant  $\beta$  subunit in *Drosophila* and the  $\beta$ PSV is only expressed in the midgut where its function is redundant with  $\beta$ PS (Devenport and Brown, 2004).

The much less genetically redundant *Drosophila* genome compared to the more complex vertebrate genome has facilitated its use in investigating the role of integrins in various biological processes. For example, by studying fly embryos that are mutant for both  $\beta$ PS and  $\beta$ PSV, it is possible to study fly development in the complete absence of integrins. The phenotypes caused by PS integrins mutations include muscles detachments, separation between

the two layers of the wing and failure in dorsal closure<sup>5</sup>. Null mutations in  $\alpha$ PS2,  $\alpha$ PS3 or  $\beta$ PS integrin subunits cause an embryonic lethal phenotype (reviewed in Brown et al. (2000)).

### 1.3.2 Talin in *Drosophila*

The *Drosophila* genome has only one talin homologue that is encoded by the *rhea* gene (Brown et al., 2002) compared to two in vertebrates (*Tln2* and *Tln1*). The *rhea* gene was identified in a screen for blisters in somatic wing clones and was named after the flightless bird rhea (Prout et al., 1997). Mutations in *rhea* cause defects in developmental processes such as germband retraction, dorsal closure, muscle detachments and wing adhesions. In *Drosophila* embryos, the *rhea* phenotype is almost identical to the phenotype caused by the absence of integrins indicating the importance of talin for integrin mediated adhesions (Brown et al., 2002). Similar to PS integrin null mutations, talin null mutation leads to an embryonic lethal phenotype (Brown et al., 2002).

### 1.3.3 The IAC in *Drosophila*

*Drosophila* has orthologs for all the major IAC components that link integrins to the cytoskeleton. This includes ILK (*ilk*) (Zervas et al., 2001), vinculin (*vinculin*) (Alatortsev et al., 1997), PINCH (*steamer duck*) (Clark et al., 2003), FAK (*DFak56*) (Grabbe et al., 2004), paxillin (*paxillin*) (Yagi et al., 2001) and tensin (*blisterly*) (Torgler et al., 2004). The phenotypes, caused by the absence of each of these proteins, reveal how important they are for integrin mediated

---

<sup>5</sup> Dorsal closure (DC) is a morphogenetic event similar to wound healing – a gap in the epithelium is closed. DC happens in late embryogenesis in *Drosophila*.

adhesions. Flies with a *vinculin* null mutation do not display any phenotype. However, flies with mutation in other genes like *ilk*, *steamer duck* and *paxillin* exhibit a subset of the phenotype caused by the absence of integrins (reviewed in Bulgakova et al. (2012)).

#### **1.3.4 Structure-function analysis of talin**

In this study, I performed structure-function analysis of talin. I used systematic approach to investigate the functional domains within the talin molecule in regards to regulation of turnover by force. My lab has generated mutations in the functional domains in *Drosophila* talin. The talin mutations that I used for this study are listed in Table 1 and displayed in Figure 4.

As mentioned previously, talin is a high molecular weight protein that interacts with multiple other adhesion proteins. Talin has two known integrin binding sites i.e. IBS-1 and IBS-2. Integrin activation is mediated through IBS-1 (see 1.2.2) (Calderwood et al., 2002) while IBS-2 has not been implicated in integrin activation. My lab has used *Drosophila* myotendinous junctions (MTJs) i.e. the muscle-tendon attachment sites as a model system, to show that IBS-2 reinforces the link between integrins and the IAC (Ellis et al., 2011). Furthermore, talin can dimerize to form an anti-parallel dimer via the dimerization domain located in the rod (Goldmann et al., 1994), the dimerization domain is also required for actin binding (Gingras et al., 2008; Smith and McCann, 2007).

**Table 1: Talin mutations used in this study.**

<b>Mutation</b>	<b>Domain</b>	<b>Molecular function</b>	<b>Reference</b>
R367A	FERM/IBS-1	blocks talin head binding to integrin cytoplasmic tail; blocks integrin activation	(Ellis et al., 2011; García-Alvarez et al., 2003; Tanentzapf and Brown, 2006)
K2094D/S2098D	IBS-2	prevent IBS-2 binding to membrane proximal domain of $\beta$ -integrin	(Ellis et al., 2011; Moes et al., 2007; Rodius et al., 2008)
L334R	FERM/IBS-1	blocks integrin activation but not talin head binding to integrin cytoplasmic tail	(Haling et al., 2011)
K2450D/V2451D/ K2452D	actin-binding domain	reduced actin binding by talin	(Franco-Cea et al., 2010; Gingras et al., 2009)

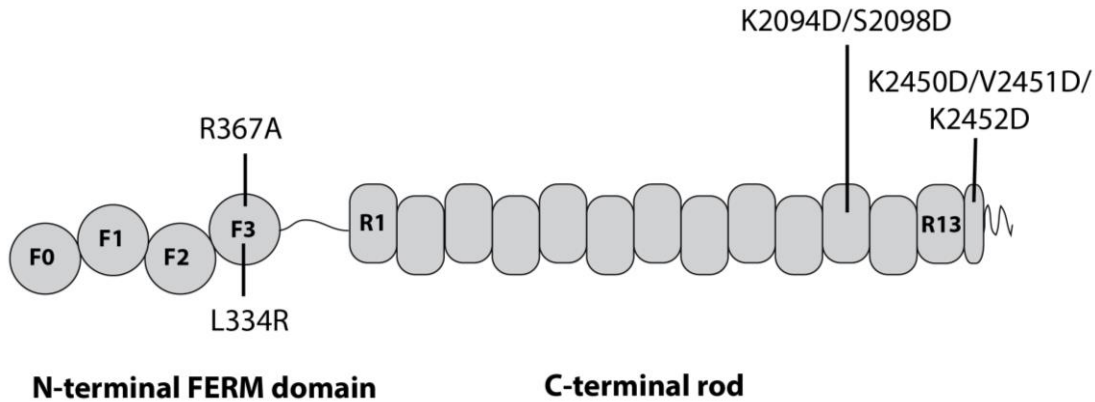


**Figure 4: Schematic of the localization of the talin mutants used in this study.**

### 1.3.5 The MTJs in *Drosophila* as a model to study cell-ECM adhesions

Throughout this study, I use the *Drosophila* MTJs, the muscle-tendon attachments sites, (see schematic in Figure 5) to study cell-ECM adhesions. The MTJs are feasible for this study for several of reasons. First, integrins and the IAC strongly localizes to the MTJs. Secondly, the

MTJs are thin and close to the epidermis of the embryo which is required for our experimental setup. Furthermore, the MTJs form linear adhesions sites that facilitate imaging.

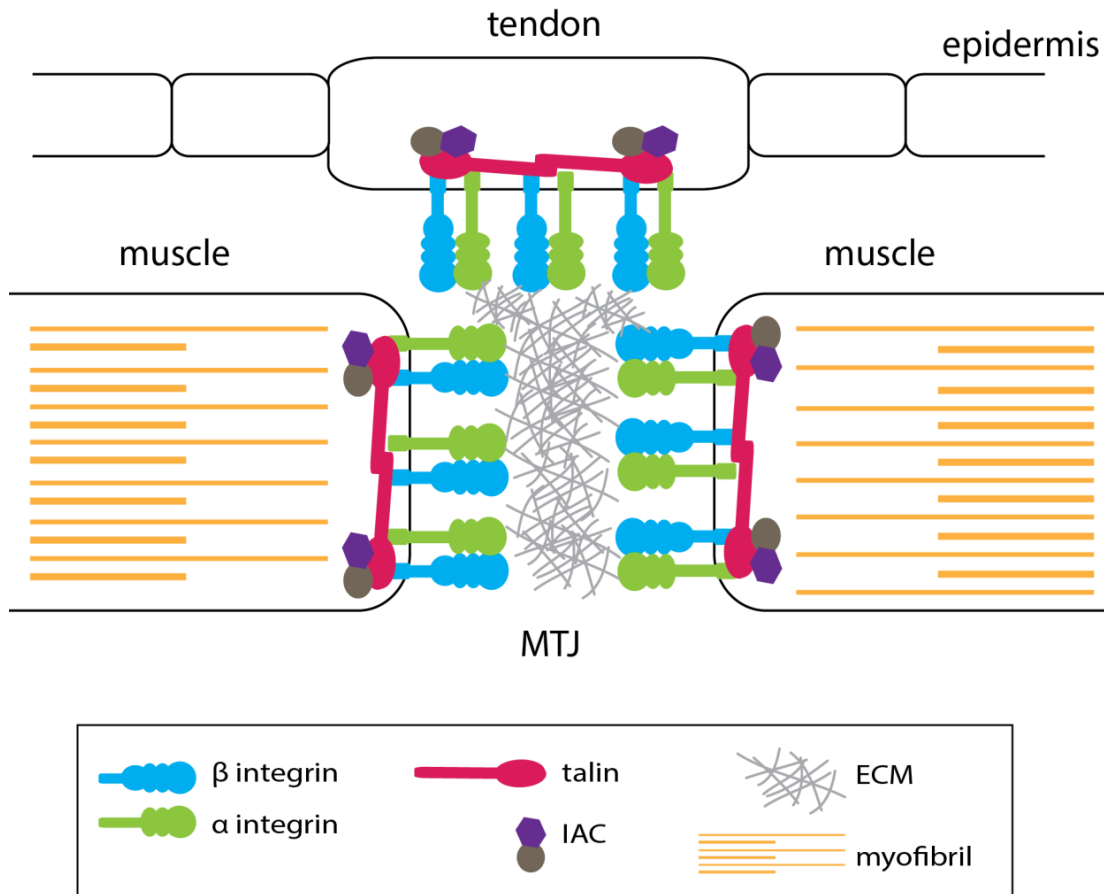


**Figure 5: Schematic of the MTJs, the muscle-tendon attachments sites in *Drosophila*.**

#### **1.4 Turnover of integrins and the IAC components**

Integrin mediated cell-ECM adhesions are dynamic and undergo constant turnover. Turnover is the process of regulated assembly and disassembly of the adhesion complex at the cell surface. Adhesion turnover involves the delivery and the removal of integrin heterodimers from the plasma membrane. Additionally, adhesion turnover involves the binding and unbinding of cytoplasmic components to the adhesion complex (Bretscher, 1989; Bretscher, 1992; Pines et al.,

2012; Wolfenson et al., 2009; Yuan et al., 2010). In the following sections, I will go over the discovery of turnover and the major molecular pathways responsible for turnover of integrins and the IAC components. In 1.4.4 and 1.4.5, I will discuss my experimental set-up and methodology in order to study protein turnover *in vivo* in response to altered force.

### **1.4.1 Studies in cell culture**

In late 1980s, Mark Bretscher first observed that integrins were internalized into the cytoplasm and subsequently exocytosed or recycled back to the cell surface. The internalization and recycling of protein molecules is referred to as protein turnover. Bretscher's work on cultured CHO (Chinese hamster ovary) cells demonstrated that integrins participate in the endo-exocytic cycle (Bretscher, 1989; Bretscher, 1992). Furthermore, his work demonstrated that the endo-exocytic cycle is a selective process where certain integrin heterodimers are rapidly recycled while others remain at the plasma membrane (Bretscher, 1992).

Subsequently, a number of FRAP (fluorescence recovery after photobleaching) studies in cultured cells have confirmed that integrins and the IAC components undergo turnover. Moreover, these studies have sought to characterize turnover kinetics in details. For example, Ballestrem et al. showed that  $\beta$ 3-integrin in migrating B16F1<sup>6</sup> cells are highly dynamic at transient adhesions at both high and low density of FA (Ballestrem et al., 2001). Another study used FRAP on HeLa cells in a combination with mathematical modelling. The authors proposed that the IAC components vinculin and paxilin would reside within three spatial domains

---

<sup>6</sup> Mouse melanoma cell line.

(cytoplasm, juxtamembrane domain<sup>7</sup> and FA) and each domain would have distinct molecular dynamics in terms of protein turnover rate (Wolfenson et al., 2009). The same research group showed that inhibition of actomyosin contractility by blebbistatin in HeLa cells has different effects on individual FA proteins. The mobile fraction of vinculin increases in response to force reduction while the mobile fraction of zyxin and paxillin decrease (Wolfenson et al., 2011). In a related study, the Rho kinase inhibitor Y-27632 was used to block the actomyosin contractility in HeLa cells. FRAP assay was performed on GFP-tagged VASP, zyxin, paxillin, vinculin, talin, kindlin 2, ILK and FAK prior to and a few minutes after treatment with Y-27632. In summary, the eight FA proteins tested responded differently to the drug. The mobile fraction of talin, VASP and FAK were not affected by Y-27623 treatment while vinculin and kindlin-2 displayed increased mobile fraction and paxillin and zyxin displayed decreased mobile fraction. In addition, for all of these FA proteins the  $k_{on}$  value (protein association rate) was higher than the  $k_{off}$  value (protein disassociation rate) in untreated cells. However, in Y-27623 treated cells the  $k_{off}$  value was higher than the  $k_{on}$  value for all of these FA proteins. This suggests that there is a net-disassociation of each of the FA proteins tested when cells are in a “relaxed state” (Lavelin et al., 2013).

#### **1.4.2 Role of the endocytic machinery in turnover**

The majority of the knowledge on the role of the endocytic machinery in integrin turnover comes from studies in migrating cells as it requires the assembly and disassembly of the adhesion complex. Many integrin heterodimers are endocytosed via clathrin-dependent mechanism. The

---

<sup>7</sup> The region surrounding the FA.

cytoplasmic tail of  $\beta$ -integrins contain conserved NXXY<sup>8</sup> motifs that are required to recruit integrins to clathrin-coated structures (CCSs) through interaction with various adaptor proteins (reviewed in (Caswell et al., 2009)). HAX1<sup>9</sup> is an example of adaptor or bridging proteins that associates with the NXXY motif in  $\beta$ -integrins. This association is required for  $\beta$ V $\beta$ 6 integrin internalization in cultured oral squamous carcinoma cells (Ramsay et al., 2007). In rare cases, no adaptor protein is needed as the cytoplasmic sequence of the integrin heterodimer associates directly with the clathrin treskelions (De Deyne et al., 1998).

In addition, some integrin heterodimers may be endocytosed via clathrin-independent routes for instance via lipid raft mediated protein trafficking. For example, antibody-induced clustering of  $\alpha$ 2 $\beta$ 1 integrin in SAOS cells (human osteosarcoma cells) redistributed  $\alpha$ 2 $\beta$ 1 from lipid rafts to caveolae where it is subsequently internalized (Upla et al., 2004). Another evidence of clathrin-independent integrin endocytosis is that down-regulation of caveolin-1 expression by siRNA markedly reduces  $\beta$ 1-integrin endocytosis (Shi and Sottile, 2008). Furthermore,  $\alpha$ v $\beta$ 3 and  $\alpha$ 5 $\beta$ 1 integrins have been shown to associate with caveolin-1 (reviewed in Caswell and Norman (2006)). It is clear that some integrins can follow both clathrin-dependent and clathrin-independent internalization routes (reviewed in Caswell et al. (2009)).

Following endocytosis, integrins are delivered to early endosomes (EEs). In EEs, a decision will be made whether integrins undergo degradation or be recycled (exocytosed) back to the plasma membrane (reviewed in (Caswell and Norman, 2006; Caswell et al., 2009)). The majority of

---

<sup>8</sup> Asparagine-X-X-Tyrosine. X donates any amino acid.

<sup>9</sup> Alternative name: HS1-associated protein X-1

internalized integrin heterodimers are rapidly recycled back to the plasma membrane (Bretscher, 1989). The Rab family of small GTPase plays an important role in vesicular trafficking and ensuring that cargos are delivered to their correct destinations (reviewed in (Caswell and Norman, 2006; Stenmark, 2009). Rab4-dependent recycling returns integrins from the EEs back to the plasma membrane without transiting through the PNCR (perinuclear recycling compartment). This is called “short loop” pathway. In contrast, Rab11-dependant integrin recycling is called “long loop” pathway and involves transiting through the PNCR before integrins are delivered to the plasma membrane (reviewed in Bridgewater et al. (2012)).

Rab21 has both been implicated in internalization and recycling of integrins. Rab21 associates with the cytoplasmic domain of the  $\alpha$ -integrin subunit and its expression induces bidirectional movement of  $\beta$ 1-integrin-containing vesicles (Pellinen et al., 2006). Other members of the Rab protein family that are thought to have a role in integrin recycling include Rab5 and Rab25 (reviewed in Caswell et al. (2009)).

### **1.4.3 Studies in *Drosophila***

Ongoing turnover of integrins and the IAC are required for transient or short term cell-ECM adhesions. Transient cell-ECM adhesions play an important role in dynamic processes such as cell migration. For example, disrupting turnover by inhibiting dynamin mediated endocytosis results in defective cell migration (Ezratty et al., 2005).

In 2009, my lab addressed the question if integrins and the IAC would also undergo turnover in long-lasting adhesions. My lab found out using FRAP assay that once assembled, the IAC undergoes turnover in long lasting cell-ECM adhesions at the MTJs in *Drosophila* larvae and

embryos. Secondly, by performing FRAP on 3rd instar larval flat preparations treated with inhibitors of clathrin (dynasore and CPZ<sup>10</sup>), my lab found out that clathrin mediated endocytosis is required for IAC and integrin turnover at the MTJs. Lastly, the results showed that the Rab family of GTPases regulates the turnover of IAC and integrins at the MTJs (Yuan et al., 2010). This was the first study where the turnover of integrins and the IAC were analyzed in intact and live animals.

In a subsequent study, my lab investigated the role of force on integrin turnover at the MTJs in *Drosophila* larvae and embryos. My lab found out using FRAP in a combination with mathematical modelling that force regulates integrin turnover. The main results were that increased force seems to stabilize cell-ECM adhesions as supported by decrease in integrin turnover. We also identified several domains within the integrin heterodimer that seem to be required for force sensing at the MTJs. For example, a mutation in the ECM binding domain (S196>F in *Drosophila*  $\beta$ PS integrin) that prevents integrin from undergoing a ligand-induced conformational changes required for outside-in signaling seems to disrupt force sensing. Increased force did not decrease integrin turnover in embryos with this mutations as compared to WT embryos (Pines et al., 2012). My project is an extension of the two studies outlined above where I continued to investigate the role of force on IAC turnover (with focus on talin).

---

<sup>10</sup> CPZ - chlorpromazine

#### 1.4.4 Regulation of talin turnover by force

To study the regulation of talin turnover by force, I use two temperature sensitive mutations that modulate the amount of force that acts on the MTJs by changing the frequency and the intensity of muscle contraction. A mutation in the gene *Breakdance* (allele *Brkd<sup>J29</sup>*) (Montana and Littleton, 2004) causes the muscles to contract with higher frequency than WT (wild type) muscles. A mutation in the gene *paralytic* (allele *para<sup>ts2</sup>*) which encodes for the voltage gated sodium channel (Grigliatti et al., 1972; Sanyal et al., 1999) almost completely inhibits muscle contraction by abrogating action potentials in motor neurons (Pittendrigh et al., 1997). My lab has physiologically confirmed the effects of the *Brkd<sup>J29</sup>* and *para<sup>ts2</sup>* mutants by monitoring the muscle contraction frequency in third instar larvae (Pines et al., 2012).

In this project, FRAP (Figure 6) is the method of choice to measure the mobile fraction of various talin mutants at the MTJs in response to modulated force. The mobile fraction provides a measure of the proportion of proteins that are freely mobile i.e. undergoing turnover at the MTJs. In general, high mobile fraction reflects more dynamic, less stable adhesions and a low mobile fraction reflects a less dynamic, more stable adhesions (Yuan et al., 2010).

FRAP experimental setup is based on genomically tagging the protein of interest (e.g. talin) with GFP (green fluorescent protein) and measuring its mobile fraction *in vivo*. A FRAP experiment involves photobleaching the region of interest (ROI) by briefly exposing it to a high-intensity laser (Reits and Neefjes, 2001). The recovery of the movement of the fluorescent protein molecules as they move into the bleached region is recorded over time. FRAP data is generally plotted as a curve, with time on the x axis and the fluorescence intensity on y-axis. Mobile fraction, which represents the total percentage of the protein that is mobile can be obtained from FRAP analysis

(Figure 6). I can assess the effect of modulated force on talin turnover by performing FRAP assay on embryos/larvae that co-express talinGFP and paralytic/Breakdance mutations.

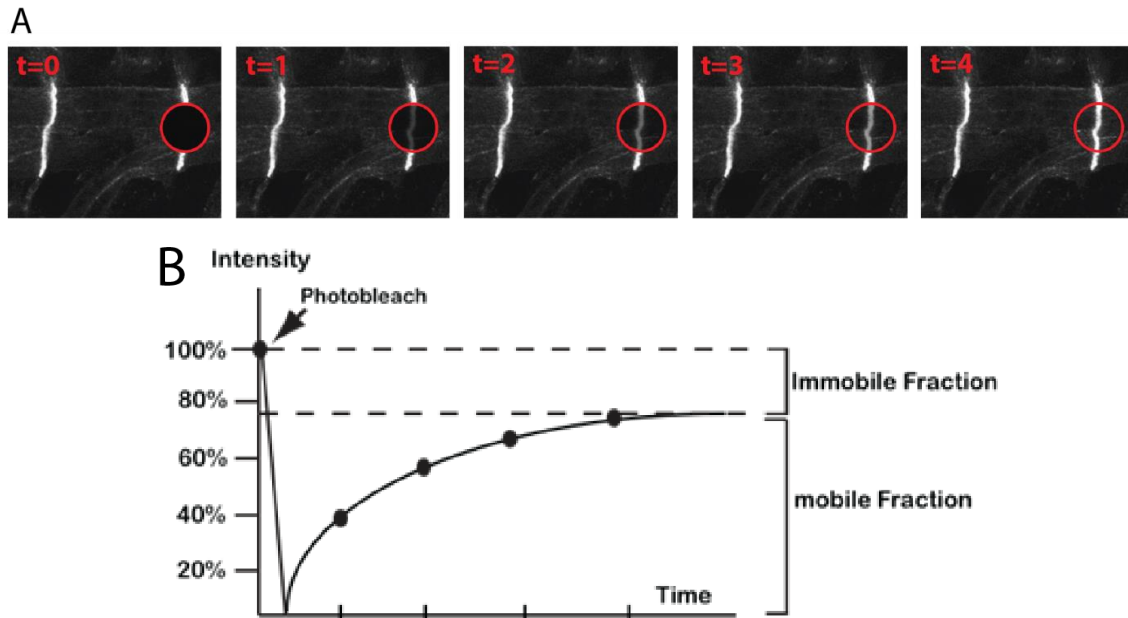


**Figure 6: FRAP (fluorescence recovery after photobleaching).**

A) GFP tagged talin localizes to the MTJs in live embryo. After bleaching (at t=0) the recovery is monitored over time (t=1-4) to obtain a FRAP recovery curve that gives the mobile fraction (MF).

B) FRAP recovery curve.

#### 1.4.5 Rate constants to describe the turnover of the adhesion proteins

In 2012, my lab modelled integrin fluorescence recovery curves to gain mechanical insight into the turnover kinetics in response to force. We modeled the fluorescence recovery of the integrins by using ordinary differential equations (ODE). The model is parameterized by two rate constants i.e.  $k_{\text{endocytosis}}$  which describes the endocytic removal of integrins from the membrane and  $k_{\text{exocytosis}}$  which describes integrin delivery to the membrane by the endocytic pathway (Pines et al., 2012).

In this study, we expanded this model for membrane proteins (integrins) to cytoplasmic proteins (talin). For cytoplasmic proteins, we also have to account for protein binding/unbinding to the adhesion complex at the plasma membrane.  $K_{on}$  describes talin binding to the adhesion complex at the plasma membrane while  $k_{off}$  describes talin unbinding the adhesion complex at the plasma membrane.  $K_{assembly}$  (abbreviated  $k_{asm}$ ) describes talin delivery to the plasma membrane due to the assembly of the adhesion complex.  $K_{disassembly}$  (abbreviated  $k_{dis}$ ) describes talin removal from the plasma membrane due to the disassembly of the adhesion complex. This is illustrated in Figure 7. Therefore, we need to model the recovery using a system of ordinary differential equations to solve for four rate constants.

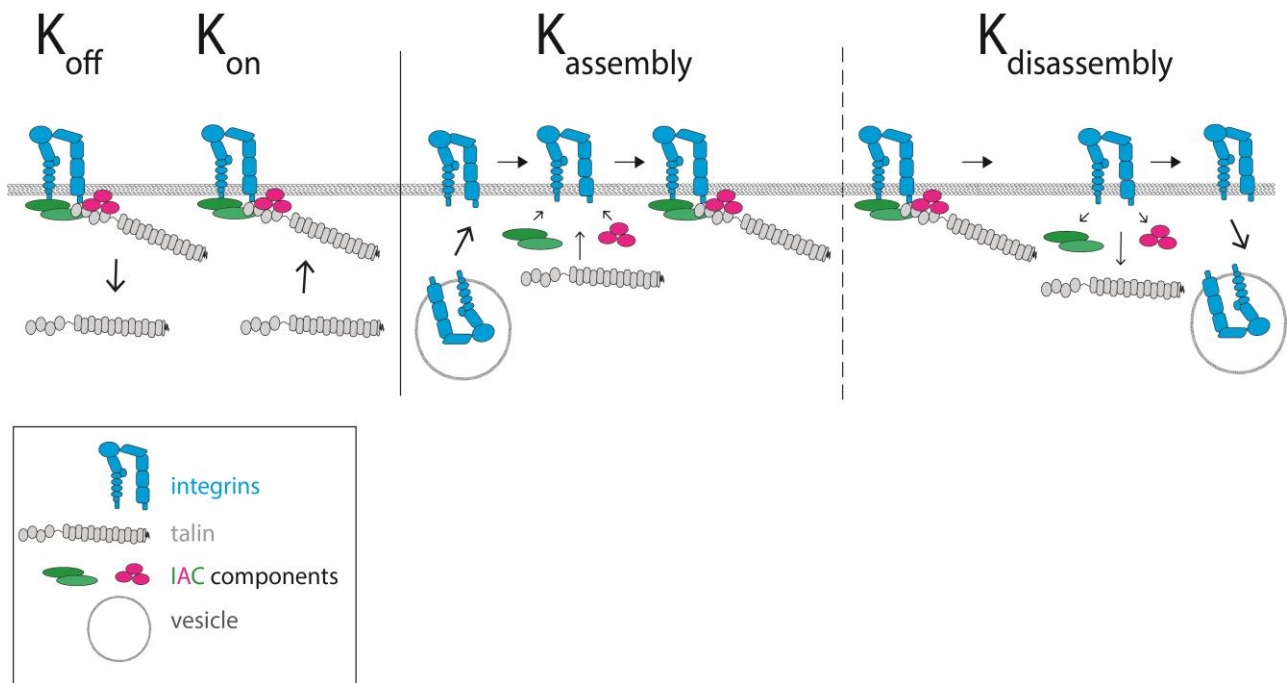


**Figure 7: Schematics of the cytoplasmic model for talin.**

The cytoplasmic model for talin is parameterized by four rate constants.

## **1.5 Objectives, rationale and hypotheses**

This research project was designed as a continuation of previous work in my lab where the turnover of integrins and the IAC has been studied (Pines et al., 2012; Yuan et al., 2010). This thesis aims to report the methodology, results and conclusions of this work.

### **1.5.1 Objective**

My overall objective is to investigate the turnover of talin at the IAC, at the MTJs in *Drosophila* embryos and larvae, in response to changes in mechanical force.

### **1.5.2 Hypothesis**

I hypothesize that talin acts as a mechanosensor – changes in force will affect talin turnover and consequently the stability of the IAC. Furthermore, I hypothesize that certain functional domains within talin are required for sensing force at the MTJs in *Drosophila* embryos and larvae.

### **1.5.3 Rationale**

- 1) My lab has shown that talin and other components of the IAC undergo turnover *in vivo* at the muscle-tendon attachments at the MTJs in live *Drosophila* (Pines et al., 2012; Yuan et al., 2010).
- 2) My lab has shown that force regulates the turnover of integrin (Pines et al., 2012). Integrin binds to talin at the IAC (Calderwood et al., 1999) and therefore I hypothesize that force also regulates the turnover of talin.

3) Mechanical force can alter the conformation of talin and thereby regulate its ability to bind to other proteins (del Rio et al., 2009). Talin is a large protein composed of several helical bundles (Goult et al., 2013). Del Rio et al. showed that when force is applied on a single talin molecule some of the bundles unfold, resulting in exposure of cryptic vinculin binding sites that are normally buried inside the molecule (del Rio et al., 2009). Therefore, I postulate that force can affect talin turnover perhaps by changing its ability to bind to other proteins.

## Chapter 2: MATERIALS AND METHODS

### 2.1 Fly stocks and lines

To visualize talin for FRAP experiments, GFP tagged talin transgenes were expressed under a ubiquitous promoter in *Drosophila* flies in WT background. All of the GFP tagged talin transgenes used in this study are published. Generation of:

- pUBI-talinEGFP is described in Yuan et al. (2010).
- pUBI-talinEGFP\* K2450D/V2451D/K2452D are described in Franco-Cea et al. (2010)
- pUBI-talinEGFP\* K2094D/S2098D is described in Ellis et al. (2011)
- pUBI-talinEGFP\*R367A is described in Ellis et al. (2011) and Tanentzapf and Brown (2006)
- pUBI-talinEGFP\*L334R is described in Ellis et al. (2014)

The mutations  $Brkd^{J29}/TM3$  and  $para^{ts2}$  were used to alter the force that acts on the MTJs in embryos and larvae.  $Brkd^{J29}/TM3$  is described in (Montana and Littleton, 2004) and  $para^{ts2}$  is described in (Pittendrigh et al., 1997), and were gifts from J. Troy Littleton (MIT, USA). Stage 17 embryos heterozygous for each GFP-fluorescently tagged talin transgene that had one copy of  $Brkd^{J29}$  were selected for FRAP analysis by selecting against a fluorescent balancer. Third instar larvae (males were selected as  $para^{ts2}$  is on the X chromosome) heterozygous for each GFP tagged talin transgene that had one copy of  $para^{ts2}$  were selected for FRAP analysis. Third-instar larvae were selected for  $para^{ts2}$  analyses because the contractility phenotype was manifested at this stage.

In analysis of talin turnover in development, the talin transgenes were expressed in  $rhea^{79}$  background because the effect of development on turnover is more pronounced when only one copy of the endogenous talin is present. The  $rhea^{79}$  allele was generated by a P-element excision that covers the entire *rhea* locus (For better description see Brown et al. (2002)).

## **2.2 FRAP experiments**

### **2.2.1 Live imaging – whole mount sample preparation**

Live embryos (stages 16 and 17) expressing GFP tagged talin transgenes were collected from apple juice agar plates, dechorionated in 50% bleach for 4 minutes, washed in a steady stream of water and mounted on a glass microscope slide in 1X PBS. Live larvae (all instar larvae) expressing GFP tagged talin transgenes were washed in 1X PBS and mounted on a glass microscope slide. To minimize sample movements, mounted samples were kept in a dark box at room temperature (or in a 37°C incubator for temperature sensitive alleles) for about 1 hour prior to imaging.

### **2.2.2 Confocal microscope settings for FRAP experiments**

FRAP experiments were performed on a confocal microscope (FV1000, Olympus) with an UplanSApo60x/1.35 oil objective (Olympus). Bleaching was performed with a 473 nm laser at 5% power using the Tornado scanning tool (Olympus) for 2 seconds at 100µs/pixel. Fluorescence intensity was recorded for 825 frames, every 0.4 seconds, thereof were 75 frames taken before the bleaching event. To control for sample movement in and out of focus, a region of interest (ROI) was selected in non photobleached region. Only FRAP curves where the fluorescence intensity remained steady throughout the whole experiment, were used for analysis.

### **2.2.3 Temperature sensitive sample preparation**

To study the temperature sensitive alleles, *para*<sup>ts2</sup> (Grigliatti et al., 1972; Sanyal et al., 1999) and *Brkd*<sup>J29</sup> (Montana and Littleton, 2004) mounted samples (temperature sensitive alleles and the respective non temperature sensitive control samples) were heat shocked at 37°C for 1.5 hour prior to FRAP analysis. Samples were kept in a Tokai Hit stagetop incubator (made by Tokai Hit Ltd, Japan) to maintain the correct temperature during imaging.

### **2.2.4 Inhibition of endocytosis in live embryos**

The drug permeabilization protocol by Schulman et al. (2013) was performed to induce 150-200 µM dynasore solution (Sigma Aldrich) into live stage 17 embryos to inhibit endocytosis. Embryos were collected from apple juice agar plates, dechorionated in 50% bleach for 4 minutes and put in a Eppendorf tube with a solution consisting of equal amounts of heptane and d-limonene (Histoclear®, National Diagnostics, HS-200, 95–100% pure D-limonene) with DMSO only (control) or dynasore dissolved in DMSO. The Eppendorf tube was placed on a rotating platform for 20 minutes. After that, the liquid was removed and samples were washed 3 times with 1X PBS. Embryos were mounted in halocarbon oil on a glass microscope slide for imaging.

## **2.3 Mathematical analysis of FRAP data**

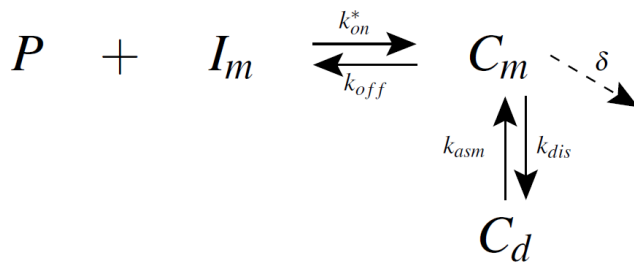
Since 2010, my lab has been collaborating with Dan Coombs' lab in the Department of Mathematics at UBC. Initially, Raibatak Das derived the mathematical model for the turnover of the adhesions proteins in *Drosophila* as outlined in Pines et al. (2012). For this project, I have been collaborating with Alejandra Herrera who has expanded the mathematical analysis to the

cytoplasmic components of the IAC and is described in the following sections. All of the mathematical analyses described below were performed in Python except the mobile fraction analysis that was performed in Matlab.

### 2.3.1 Cytoplasmic model

*[The mathematical analysis described in this chapter was developed and performed by Alejandra Herrera. More detailed mathematical description and assumptions can be seen in Appendix A]*

The new cytoplasmic model as described in 1.4.5 (illustrated in Figure 7) can be described with the following model:



This model takes into account talin's binding interaction with integrin at the membrane as well as the disassembly of IAC where

- P is free and fluorescently labeled cytosolic protein talin,
- $I_m$  is membrane protein integrin,
- $C_m$  are complex and components at the membrane
- $C_d$  are complex and components that are not at the membrane
- $K_{on}$  describes the rate of talin binding to the adhesion complex at the plasma membrane while
- $k_{off}$  describes the rate of talin unbinding the adhesion complex at the plasma membrane.
- $k_{asm}$  describes the rate of talin delivery to the plasma membrane due to the assembly of the adhesion complex while
- $k_{dis}$  describes rate of talin removal from the plasma membrane due to the disassembly of the adhesion complex
- $\delta$  is the photobleaching rate

For this model, the recovery is obtained by defining system of ordinary differential equations which can be solved for the four rate constants:

$$\begin{aligned}\frac{dC_m}{dt} &= -(k_{off} + k_{dis} + \delta)C_m + k_{on}I_mP + k_{asm}C_d \\ \frac{dP}{dt} &= -k_{on}^*I_mP + k_{off}C_m \\ \frac{dC_d}{dt} &= k_{dis}C_m - k_{asm}C_d\end{aligned}$$

For detailed derivations and initial conditions, see Appendix A.

To fit and solve FRAP data to this model, we used non-linear least square (NLLS) minimization and then we used a bootstrap resampling procedure (also described in Appendix A) to compute bootstrap distribution of each rate constant. The action of solve and fit model, and find the bootstrap distribution will be denoted as “simple fit”.

### 2.3.2 Double fitting to derive rate constants

*[The mathematical analysis described in this chapter was developed and performed by Alejandra Herrera. More detailed mathematical description and assumptions can be seen Appendix A]*

By using FRAP data only and the differential equations discussed above, it is not possible to distinguish between the two rate constants that contribute to talin delivery to the plasma membrane ( $k_{asm}$  and  $k_{on}$ ) and the two rate constants that contribute to talin removal from the plasma membrane ( $k_{dis}$  and  $k_{off}$ ). This creates an inherent symmetry in the model system.

To solve this problem, we perform additional FRAP experiments with the endocytosis inhibitor dynasore (Macia et al., 2006). It has been shown that endocytosis has a role in the disassembly of the IAC (Ezratty et al., 2009). Therefore, we assume by inhibiting endocytosis (with

dynasore), we are mostly affecting the disassembly process ( $k_{\text{dis}}$  decreases) while other processes ( $k_{\text{on}}$ ,  $k_{\text{off}}$  and  $k_{\text{asm}}$ ) remain the same. We performed the drug permeabilization protocol by Schulman et al. (2013) to introduce the endocytosis inhibitor dynasore into stage 17 embryos (as outlined in 2.2.4). We did this for embryos expressing GFP tagged talin transgenes (WT talin and all talin mutants that were tested). For the control experiment, we performed exactly the same procedure except no dynasore was in the permeabilization solution. The results from these experiments are in Appendix B

The experiments outlined above, enable us to distinguish the correct value of each rate constant as we can assume that the only difference between the dynasore and the control dataset lies in  $k_{\text{dis}}$ . This is done by using a “double fitting” method which refers to solve, fit and calculate bootstrap distribution simultaneously for the control and dynasore data where  $k_{\text{on}}$ ,  $k_{\text{off}}$ ,  $k_{\text{asm}}$  are assumed the same for both datasets, but  $k_{\text{dis}}$  is different.

For each dataset of interest (i.e. WT talin and talin mutants in  $\text{Brkd}^{\text{J29}}/\text{para}^{\text{ts2}}$  background), the “double fitting” approach is used; the simple fit bootstrap distribution of the dataset of interest is compared to the double fit distribution, and the range of the simple fit distribution is selected which is closest to the double fit distribution. The selected simple fit distribution for each rate constant is then used to establish whether rate constants showed statistically significant differences between two experiments of interest (see Figure 8 for further clarification).

Hence, we use the double fitting results from stage 17 embryos (i.e. dynasore dataset) to determine the true bootstrap distribution for datasets for third instar larvae. This is done because the permeabilization protocol by Schulman et al. (2013) that we use in the dynasore experiments only works for embryos.

### 2.3.3 Mobile fraction analysis

*[The mathematical analysis described in this chapter was performed by Walter Wasserman and Katie Goodwin.]*

Mobile fraction was determined by the following equation:

$$f(t) = f_{max}(1 - e^{-t/\tau})$$

where  $f(t)$  is the fluorescence recovery,  $t$  is time and  $f_{max}$  and  $\tau$  are fitting parameters. The parameter  $f_{max}$  is the maximal mobile fraction and  $\tau$  is a constant that is related to the rate of the recovery (i.e. the shape of the FRAP curve). Non-linear least square fitting was performed for all replicates in an experiment. The final mobile fraction for each experiment was calculated by averaging  $f_{max}$  for all the replicates in a corresponding experiment.

## Chapter 3: RESULTS

### 3.1 Developing a model for the turnover of cytoplasmic proteins

*[The mathematical analysis described in this chapter was developed and performed by Alejandra Herrera. More detailed mathematical description and assumptions can be seen Appendix A]*

Figure 8 illustrates all the steps taken in the mathematical analysis (see 2.3.1 and 2.3.2) to characterize the turnover of cytoplasmic proteins. This procedure was used to derive rate constants (and its confidence intervals) for all the experiments which are displayed in Figure 9 to Figure 13 (for parameter estimates and final bootstrap distribution values, see Appendix C).

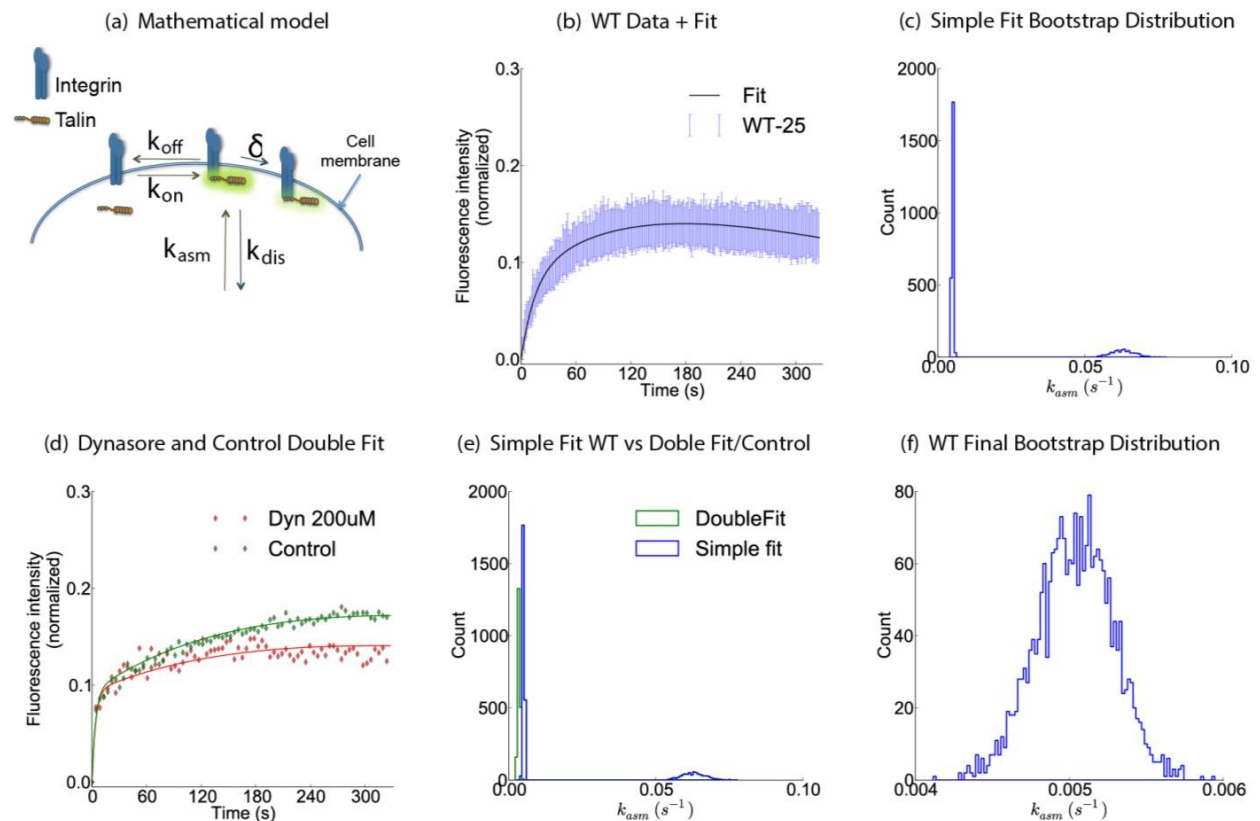


**Figure 8: Development of the mathematical model to characterize turnover for cytoplasmic proteins.**

**Figure 8. Development of the mathematical model to characterize turnover for cytoplasmic proteins [Figure created by Alejandra Herrera].** An illustration showing all the steps of the mathematical analysis for a typical FRAP dataset (this example is based on FRAP data for talin tagged with GFP in a WT background for embryonic stage 17 embryos at 25°C).

(a) The mathematical model of cytoplasmic proteins is characterized by four rate constants ( $k_{on}$ ,  $k_{off}$ ,  $k_{dis}$  and  $k_{asm}$ ).

(b) As a first step, each FRAP dataset of interest (e.g. talin in Brkd<sup>J29</sup>/para<sup>ts2</sup> background) is fitted to the cytoplasmic model (2.3.1). We call this regression ‘simple fit’. Error bars indicate SEM.

(c) After a FRAP dataset has been fitted, bootstrap distribution is calculated for all rate constants. The simple fit bootstrap distribution yields bimodal distribution due to the inherent symmetry in the model (discussed in 2.3.2). In this example, it can be seen that  $k_{asm}$  distribution has two peaks.

(d) Dynasore dataset and corresponding control dataset are fitted to the model. ‘Double fit’ refers to solve and fit, and find parameter confidence intervals simultaneously for these data sets.

(e) The double fitting approach gives us the double fit distribution of each rate constant (green colour) which is compared to the simple fit bootstrap distribution of the same rate constant (blue colour, same as in [c]). The simple fit bootstrap distribution peak which is closest to the double fit distribution range is selected.

(f) The selected bootstrap distribution peak is considered the final distribution of a rate constant for the simple fit dataset. This example shows the final bootstrap distribution for  $k_{asm}$ . The bootstrap can then be used to compute the 95% confidence interval for the  $k_{asm}$  rate constant.

### 3.2 Analysis of talin turnover in response to altered force

To analyse the turnover of WT talin and talin mutants (see Table 1 for talin mutants), I performed FRAP on the MTJs in intact and live *Drosophila melanogaster* embryos and larvae expressing GFP-tagged talin transgenes (see 1.4.4 for explanation of FRAP, Figure 6 for schematic of FRAP and Figure 5 for schematic of the MTJs). To investigate talin turnover in response to increased and decreased force I modulated the force that acts on the MTJs by expressing the temperature sensitive alleles *Brkd<sup>J29</sup>* and *para<sup>ts2</sup>* in embryos and larvae (see 1.4.4 for explanation of *Brkd<sup>J29</sup>* and *para<sup>ts2</sup>*). Because certain temperature (37°C) is required to trigger the *Brkd<sup>J29</sup>* and *para<sup>ts2</sup>* phenotype, I have to control for the temperature by performing the same experiment at room temperature (25°C).

As discussed earlier, definitions of each rate constants are as follows:

- **k<sub>asm</sub>**: talin delivery to the plasma membrane due to the assembly of the adhesion complex.
- **k<sub>dis</sub>**: talin removal from the plasma membrane due to the disassembly of the adhesion complex.
- **K<sub>on</sub>**: talin binding to the adhesion complex at the plasma membrane
- **k<sub>off</sub>**: talin unbinding the adhesion complex at the plasma membrane

(See Figure 7 for clarification).

We used the methodology outlined in section 3.1 above to compute the 95% confidence interval for each rate constant, and to establish whether the rate constant estimates showed statistically significant differences between experiments at 25°C and 37°C.

To facilitate data interpretation, I calculated the relative changes in rate constants from 25°C to 37°C using the following formula:

$$\text{Relative change} = \frac{k_x^{37^\circ\text{C}} - k_x^{25^\circ\text{C}}}{k_x^{25^\circ\text{C}}}$$

where  $k_x^{25^\circ\text{C}}$  is a rate constant  $x$  at  $25^\circ\text{C}$  and  $k_x^{37^\circ\text{C}}$  is a rate constant  $x$  at  $37^\circ\text{C}$ .

By calculating relative changes in rate constants, I can evaluate how increased force (allele *Brkd<sup>J29</sup>*) or decreased force (allele *para<sup>ts2</sup>*) affects individual rate constants. Furthermore, by comparing relative change of different rate constants, I can gain mechanistic insight into talin turnover.

In addition, I calculated rate constant ratios  $\frac{k_{off}}{k_{on}}$  and  $\frac{k_{asm}}{k_{dis}}$  at  $25^\circ\text{C}$  and  $37^\circ\text{C}$ .

By calculating rate constant ratios, I can evaluate how increased force (allele *Brkd<sup>J29</sup>*) or decreased force (allele *para<sup>ts2</sup>*) affects the relationship between  $k_{asm}$  and  $k_{dis}$ , as well as,  $k_{off}$  and  $k_{on}$ .

### 3.2.1 Talin turnover in response to increased force

I measured talin turnover in response to increased force (allele *Brkd<sup>J29</sup>*) in intact and live *Drosophila melanogaster* embryos at stage 17. Embryonic stage 17 is the last embryonic stage in the development of *Drosophila melanogaster* and lasts until the hatching of the embryo.

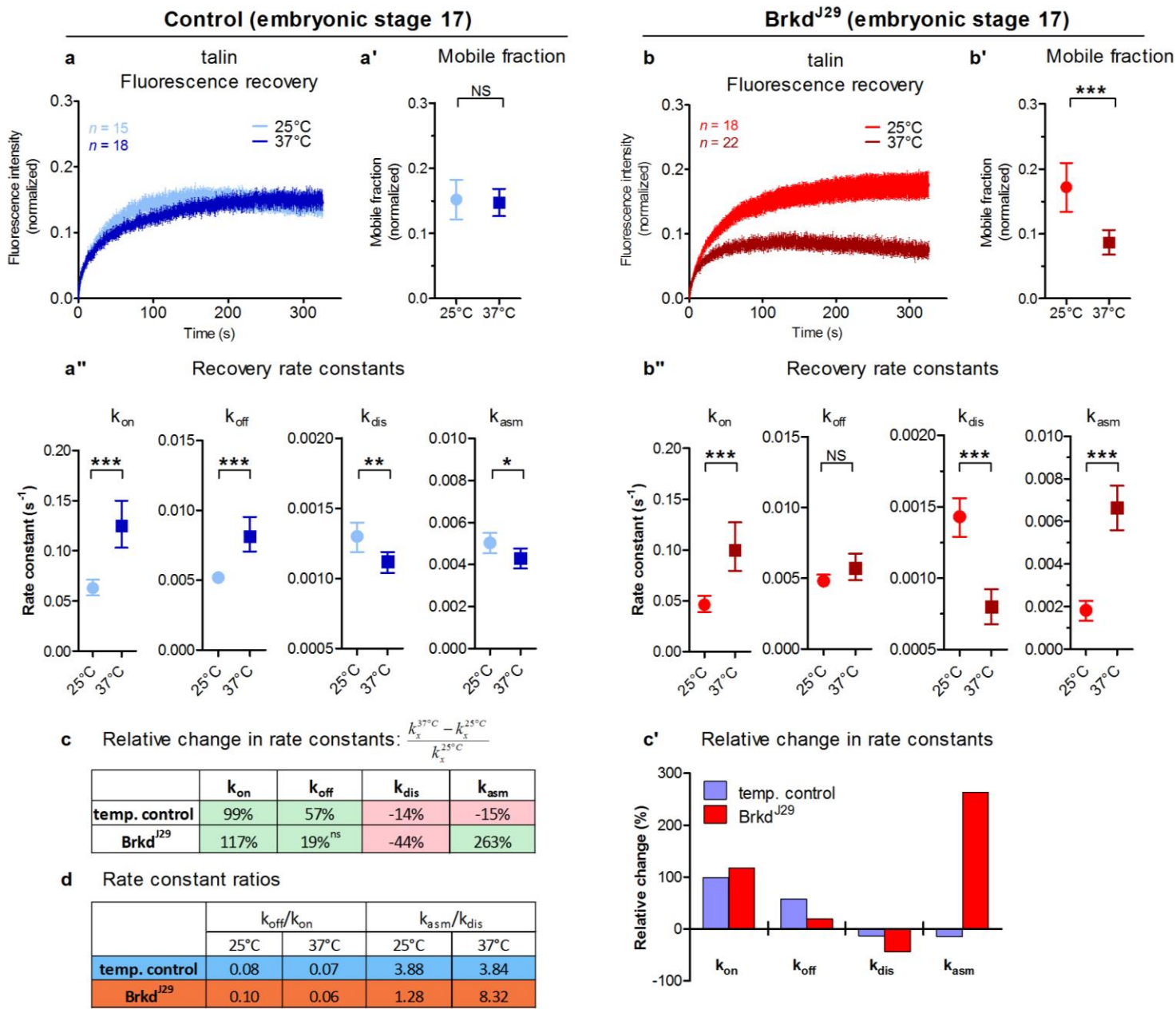


**Figure 9: Turnover of WT talin in Brkd<sup>J29</sup> background.**

**Figure 9: Turnover of WT talin in Brkd<sup>J29</sup> background.**

Blue denotes temperature control (a, a' and a''). Red denotes Brkd<sup>J29</sup> experiment (b, b' and b'').

For the temperature control experiment, 25°C and 37°C causes no changes in force. For the Brkd<sup>J29</sup> experiment, 25°C (control) causes no changes in force while 37°C causes increased force to act on the MTJs. FRAP experiments were carried out in live intact stage 17 embryos.

(a-b) FRAP curves for WT talin tagged with GFP at 25°C and 37°C in (a) WT background (temperature control) and in (b) Brkd<sup>J29</sup> background.

(a'-b') The corresponding mobile fraction values.

(a''-b'') The corresponding rate constants values.

(c) and (c') Relative change for each rate constant ( $k_x$ ) between 25°C (control [ $k_x^{25^\circ\text{C}}$ ]) and 37°C (increased force [ $k_x^{37^\circ\text{C}}$ ]). For table (c), green boxes indicate positive relative change and red boxes indicate negative relative change in rate constants. (c') shows plotted values of table (c).

(d) Rate constant ratios ( $k_{\text{off}}/k_{\text{on}}$  and  $k_{\text{asm}}/k_{\text{dis}}$ ) calculated at 25°C (control) and 37°C (increased force).

(a-b) Represent mean values  $\pm$  SEM. (a'-b') represent mean values of all FRAP curves  $\pm$  95% confidence intervals. (a''-b'') represent mean values  $\pm$  95% bootstrap confidence intervals. For all panels ns indicates a p-value  $> 0.05$ , \* indicates a p-value  $\leq 0.05$ , \*\* indicates a p-value  $\leq 0.01$ , \*\*\* indicates a p-value  $\leq 0.001$ .

Mobile fraction of WT talin (temperature control) is unaffected at 37°C when compared to 25°C indicating that elevated temperature does not affect the mobile fraction significantly (Figure 9 a'). On the other hand, WT talin in Brkd<sup>J29</sup> background responds to increased force by reduction in the mobile fraction (Figure 9 b').

Comparison of the rate constants in the temperature control (Figure 9 a') and under increased force (Figure 9 b') reveals that increased force causes dramatic increase in  $k_{asm}$  (Figure 9 b'). Furthermore, the relative change between  $k_{asm}$  at 25°C and 37°C is -15% in the temperature control but is +263% in the Brkd<sup>J29</sup> experiment (Figure 9 c and c').

In addition, it is noteworthy that there was no statistically significant change in  $k_{off}$  in response to the elevated temperature (whereas there is significant change for  $k_{off}$  for WT), suggesting an effective reduction in  $k_{off}$  (Figure 9 a' and b'). The same trend occurs for  $k_{dis}$  where there is significant change for  $k_{dis}$  in both temperature control and in the Brkd<sup>J29</sup> experiment – elevated temperature increases the relative change negatively from -14% to -44%. In contrast, for the other rate constants, increased force does not seem to affect the relative change (between 25°C and 37°C) as severely as it is similar for the temperature control and the Brkd<sup>J29</sup> experiment (Figure 9 c and c').

When comparing the rate constant ratios,  $k_{off}/k_{on}$  is similar at both temperatures for both experiments. However, when comparing  $K_{asm}/k_{dis}$ , it remains the same (~3.8) for the WT experiment at both temperatures while it increases from 1.28 at 25°C to 8.32 at 37°C (goes up by factor of nearly 7) for the Brkd<sup>J29</sup> experiment (Figure 9 d).

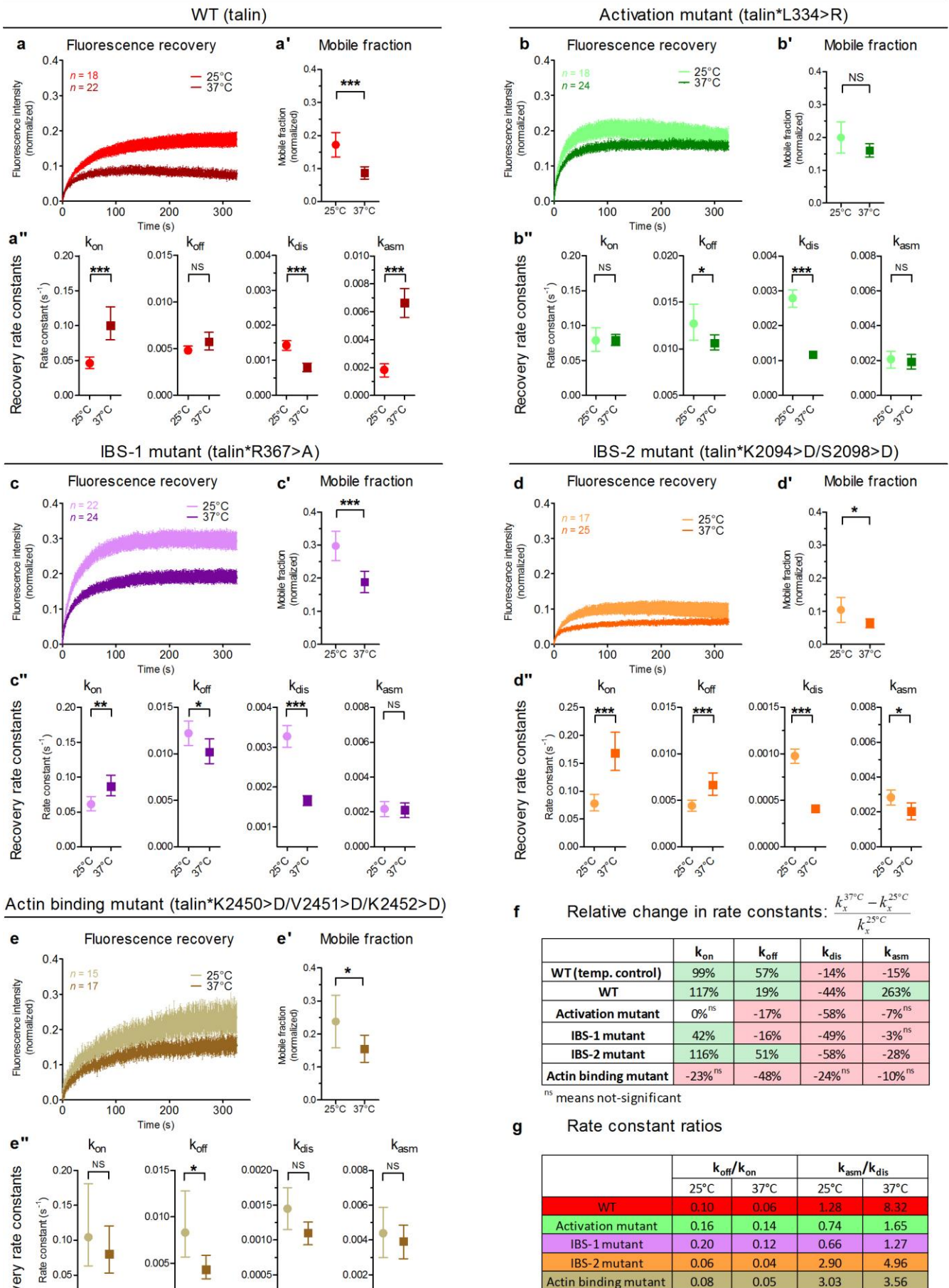


**Figure 10: Turnover of talin mutants in *Brkd<sup>J29</sup>* background.**

**Figure 10: Turnover of talin mutants in Brkd<sup>J29</sup> background.**

**Red** denotes WT talin (a, a'' and a'''). **Green** denotes activation mutant (b, b' and b''). **Purple** denotes IBS-1 mutant (c, c' and c''). **Orange** denotes IBS-2 mutant (d, d'' and d'''). **Brown** denotes actin binding mutant (e, e' and e''). For the Brkd<sup>J29</sup> experiment, 25°C (control) causes no changes in force while 37°C causes increased force to act on the MTJs. FRAP experiments were carried out in live intact stage 17 embryos.

(a-e) FRAP curves for (a) WT talin and (b-e) talin mutants, tagged with GFP in Brkd<sup>J29</sup> background at 25°C (control) and 37°C (increased force).

(a'-e') The corresponding mobile fraction values.

(a''-e'') The corresponding rate constants values.

(f) Relative change for each rate constant ( $k_x$ ) between 25°C (control [ $k_x^{25^\circ\text{C}}$ ]) and 37°C (increased force [ $k_x^{37^\circ\text{C}}$ ]). Green boxes indicate positive relative change and red boxes indicate negative relative change in rate constants.

(g) Rate constant ratios ( $k_{\text{off}}/k_{\text{on}}$  and  $k_{\text{asm}}/k_{\text{dis}}$ ) calculated at 25°C (control) and 37°C (increased force).

(a-e) Represent mean values  $\pm$  SEM. (a'-e') represent mean values of all FRAP curves  $\pm$  95% confidence intervals. (a''-e'') represent mean values  $\pm$  95% bootstrap confidence intervals. For all panels ns indicates a p-value  $> 0.05$ , \* indicates a p-value  $\leq 0.05$ , \*\* indicates a p-value  $\leq 0.01$ , \*\*\* indicates a p-value  $\leq 0.001$ .

All of the talin mutants responded to increased force in a similar way as WT talin i.e. by reduction in the mobile fraction (Figure 10 a'-e'). However, this reduction is non-significant for the activation mutant (Figure 10 b').

Interestingly, none of the talin mutants display positive relative change in  $k_{asm}$  as seen for WT talin (Figure 10 f). In other words, the relative change in  $k_{asm}$  for WT talin is +263% but varies from -28% to -3% for the mutants. In contrast, the relative change in  $k_{dis}$  is similar (negative) for both WT talin and the mutants. The relative change in  $k_{on}$  is only negative (non-significant) for the actin binding mutant. Furthermore, the relative change in  $k_{off}$  is negative for the activation mutant, IBS-1 mutant (-16%, -17% respectively) and particularly the actin binding mutant, which displays the greatest negative change (-48%) (Figure 10 f).

When comparing the rate constant ratios, it can be seen that  $k_{off}/k_{on}$  for WT talin and the talin mutants are in a very similar range for both temperatures, with  $k_{off}$  always being proportionally smaller than  $k_{on}$  at 37°C (Figure 10 g).  $k_{asm}/k_{dis}$  ratio differs for WT talin and all the mutants at 25°C as compared to 37°C, indicating that increased force affects  $k_{asm}/k_{dis}$ . It is noteworthy that  $k_{asm}/k_{dis}$  is seven times higher for WT talin but only approximately two times higher for all the talin mutants at 37°C compared to 25°C. This indicates that under increased force the  $k_{asm}/k_{dis}$  ratio is partially dysregulated in all of the mutants (Figure 10 g).

### 3.2.2 Talin turnover in response to decreased force

I measured talin turnover in response to decreased force (allele *para<sup>ts2</sup>*) in intact and live *Drosophila melanogaster* third instars. Third instar is the last larval stage before pupation.

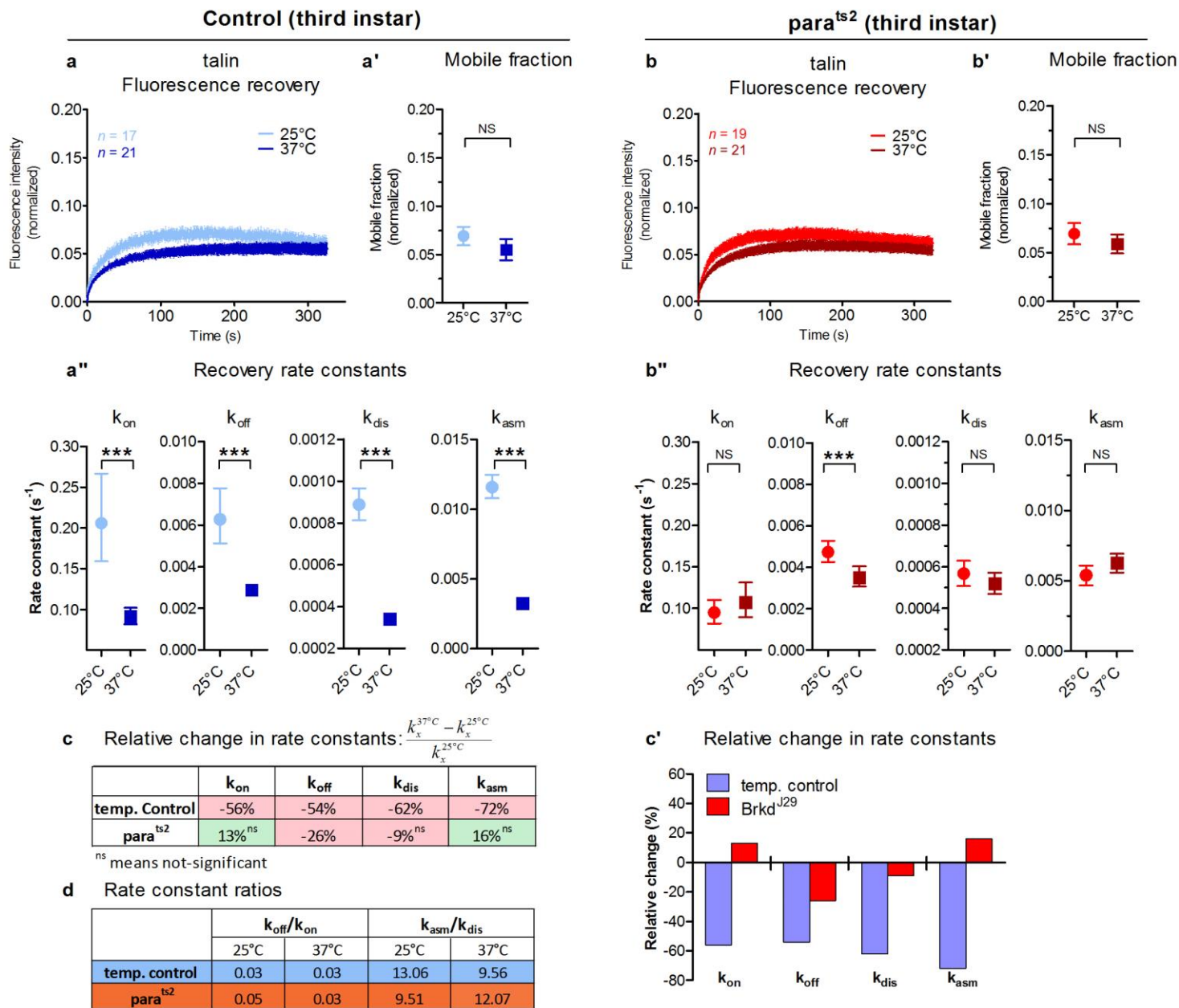


**Figure 11: Turnover of WT talin in  $para^{ts2}$  background.**

**Figure 11: Turnover of WT talin in  $para^{ts2}$  background.**

Blue denotes temperature control (a, a' and a''). Red denotes  $para^{ts2}$  experiment (b, b' and b'').

For the temperature control experiment, 25°C and 37°C causes no changes in force. For the  $para^{ts2}$  experiment, 25°C (control) causes no changes in force while 37°C causes decreased force to act on the MTJs. FRAP experiments were carried out in live third instar larvae.

(a-b) FRAP curves for WT talin tagged with GFP at 25°C and 37°C, in (a) WT background (temperature control) and in (b)  $para^{ts2}$  background.

(a'-b') The corresponding mobile fraction values.

(a''-b'') The corresponding rate constants values.

(c) and (c') Relative change for each rate constant ( $k_x$ ) between 25°C (control [ $k_x^{25^\circ C}$ ]) and 37°C (decreased force [ $k_x^{37^\circ C}$ ]). For table (c), green boxes indicate positive relative change and red boxes indicate negative relative change in rate constants. (c') shows plotted values of table (c).

(d) Rate constant ratios ( $k_{off}/k_{on}$  and  $k_{asm}/k_{dis}$ ) calculated at 25°C (control) and 37°C (decreased force).

(a-b) Represent mean values  $\pm$  SEM. (a'-b') represent mean values of all FRAP curves  $\pm$  95% confidence intervals. (a''-b'') represent mean values  $\pm$  95% bootstrap confidence intervals. For all panels ns indicates a p-value  $> 0.05$ , \* indicates a p-value  $\leq 0.05$ , \*\* indicates a p-value  $\leq 0.01$ , \*\*\* indicates a p-value  $\leq 0.001$ .

Mobile fraction of WT talin (temperature control) is unaffected at 37°C when compared to 25°C indicating that elevated temperature does not affect the mobile fraction significantly (Figure 11 a'). Furthermore, the mobile fraction of WT talin in para<sup>ts2</sup> background is non-significant at 25°C compared to 37°C, indicating that decreased force does not affect the mobile fraction (Figure 11 b').

Comparison of the rate constants in the temperature control (Figure 11 a'') reveal that elevated temperature seems to reduce all the rate constants, i.e. all rate constants for WT talin are significantly lower at 37°C compared to 25°C. However, in the para<sup>ts2</sup> experiment,  $k_{on}$ ,  $k_{dis}$  and  $k_{asm}$  become non-significant indicating an effective increase in these rate constants (compared to the temperature control). Further comparison (relative change) can be seen in Figure 11 c and c'.

When comparing the rate constant ratios,  $k_{off}/k_{on}$  is about the same for both temperatures for both experiments. However, when comparing  $k_{asm}/k_{dis}$  at 25°C and 37°C, it goes down from 13.1 to 9.6 for the control experiment, but in the para<sup>ts2</sup> experiment, it goes up from 9.5 to 12.1 (Figure 11 d).

*para<sup>ts2</sup>* (third instar)

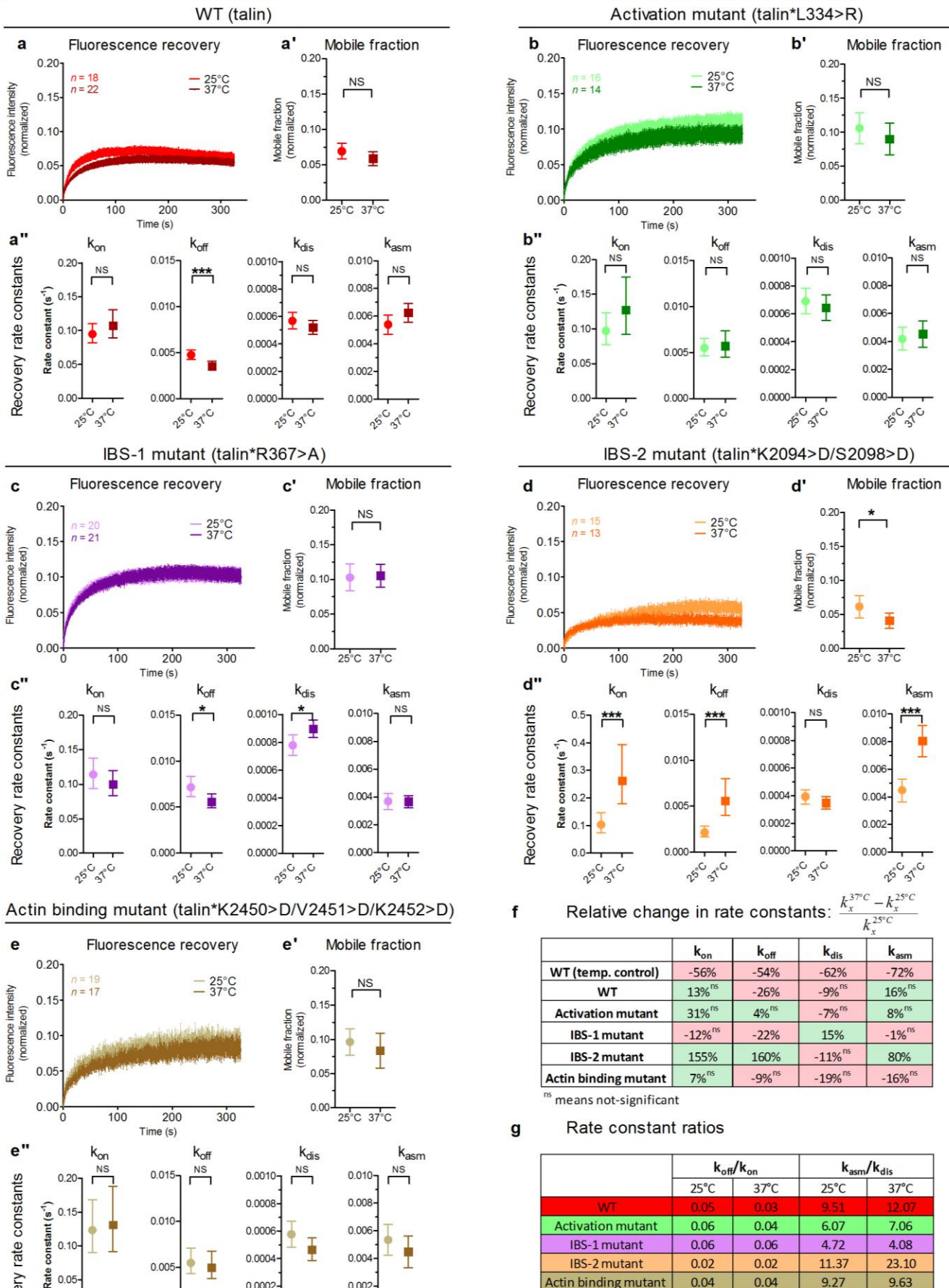


**Figure 12: Turnover of talin mutants in *para<sup>ts2</sup>* background.**

**Figure 12: Turnover of talin mutants in  $\text{para}^{\text{ts2}}$  background.**

**Red** denotes WT talin (a, a' and a''). **Green** denotes activation mutant (b, b' and b''). **Purple** denotes IBS-1 mutant (c, c' and c''). **Orange** denotes IBS-2 mutant (d, d' and d''). **Brown** denotes actin binding mutant (e, e' and e''). For the  $\text{para}^{\text{ts2}}$  experiment, 25°C (control) causes no changes in force while 37°C causes decreased force to act on the MTJs. FRAP experiments were carried out in live third instar larvae.

(a-e) FRAP curves for (a) WT talin and (b-e) talin mutants, tagged with GFP in  $\text{para}^{\text{ts2}}$  background at 25°C (control) and 37°C (decreased force).

(a'-e') The corresponding mobile fraction values.

(a''-e'') The corresponding rate constants values.

(f) Relative change for each rate constant ( $k_x$ ) between 25°C (control [ $k_x^{25^\circ\text{C}}$ ]) and 37°C (decreased force [ $k_x^{37^\circ\text{C}}$ ]). Green boxes indicate positive relative change and red boxes indicate negative relative change in rate constants.

(g) Rate constant ratios ( $k_{\text{off}}/k_{\text{on}}$  and  $k_{\text{asm}}/k_{\text{dis}}$ ) calculated at 25°C (control) and 37°C (decreased force).

(a-e) Represent mean values  $\pm$  SEM. (a'-e') represent mean values of all FRAP curves  $\pm$  95% confidence intervals. (a''-e'') represent mean values  $\pm$  95% bootstrap confidence intervals. For all panels ns indicates a p-value  $> 0.05$ , \* indicates a p-value  $\leq 0.05$ , \*\* indicates a p-value  $\leq 0.01$ , \*\*\* indicates a p-value  $\leq 0.001$ .

The mobile fraction of WT talin and the talin mutants is unaffected at 37°C (decreased force) compared to 25°C (control). Interestingly, the only exception is IBS-2 where decreased force seems to lower the mobile fraction significantly (Figure 12 a'-e').

When comparing the rate constants,  $k_{\text{off}}$  is the only rate constant for WT talin that is affected significantly by decreased force (Figure 12 a''). For the activation mutant (Figure 12 b'') and the actin binding mutant (Figure 12 e'') none of the rate constants are affected by decreased force as there was no significant change. For the IBS-1 mutant,  $k_{\text{off}}$  and  $k_{\text{dis}}$  display significant negative and positive change, respectively, in response to decreased force (Figure 12 c''). The IBS-2 mutant seems to be most affected by decreased force because  $k_{\text{on}}$ ,  $k_{\text{off}}$  and  $k_{\text{asm}}$  all display a positive significant change (Figure 12 d''). The relative change between 25°C and 37°C in rate constants is shown in (Figure 12 f). Interestingly, the IBS-2 mutant displays +155% relative change in  $k_{\text{on}}$  and +160% in  $k_{\text{off}}$  while WT displays only +13% (thus not significant) and -26% for  $k_{\text{on}}$  and  $k_{\text{off}}$ , respectively. Additionally, IBS-2 displays +80% relative change in  $k_{\text{asm}}$  while it is non-significant for WT.

The  $k_{\text{off}}/k_{\text{on}}$  ratio for WT talin and the talin mutants were very similar for both temperatures indicating that decreased force does not affect the  $k_{\text{off}}/k_{\text{on}}$  ratio (Figure 12 g). Interestingly, the  $k_{\text{asm}}/k_{\text{dis}}$  ratio goes up from 25°C to 37°C by a factor of approximately 2 (11.4 to 23.1) for the IBS-2 mutant compared to ratio only increasing from 9.5 to 12.1 in WT talin. For the rest of the mutants  $k_{\text{asm}}/k_{\text{dis}}$  ratio is similar at both temperatures, indicating that decreased force does not affect this relationship (Figure 12 g).

### 3.3 Talin turnover in development

I sought to investigate whether talin turnover is developmentally regulated i.e. if the mobile fraction and the rate constants show differences depending on the developmental stage. Therefore, I measured the turnover of WT talin in a heterozygous background (allele rhea<sup>79</sup>) in four developmental stages in *Drosophila* i.e. embryonic stage 16, embryonic stage 17, first instar larvae and third instar larvae.

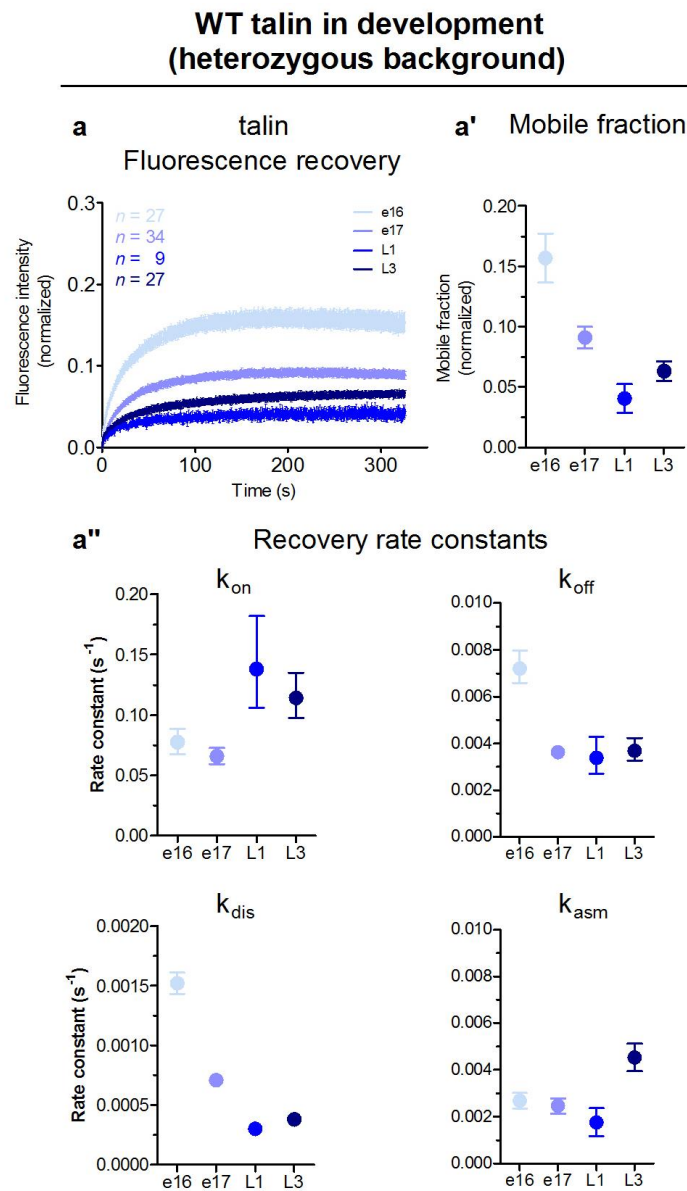


**Figure 13: Turnover of WT talin in development (heterozygous background).**

**Figure 13: Turnover of WT talin in development (heterozygous background).**

(a) FRAP curves for WT talin tagged with GFP in heterozygous background for progressive developmental stages i.e. embryonic stages 16 and 17 (denoted e16 and e17) and first and third instar larvae (denoted L1 and L3).

(a') The corresponding mobile fraction values.

(a'') The corresponding rate constants values.

(a) Represent mean values  $\pm$  SEM. (a') represent mean values of all FRAP curves  $\pm$  95% confidence intervals. (a'') represent mean values  $\pm$  95% bootstrap confidence intervals. For all panels ns indicates a p-value  $> 0.05$ , \* indicates a p-value  $\leq 0.05$ , \*\* indicates a p-value  $\leq 0.01$ , \*\*\* indicates a p-value  $\leq 0.001$ .

The mobile fraction displays an obvious decrease between stages 16 and 17. However, between first- and third instar it displays a slight increase (Figure 13 a').

The rate constant analysis reveals that  $k_{on}$  is higher in larvae compared to embryos.  $K_{off}$  is highest in embryonic stage 16 and displays similar values for embryonic stage 17 and the two larval stages.  $K_{dis}$  is higher in embryos compared to larvae.  $K_{asm}$  is highest in third instar larvae but displays similar values for the embryonic stages and the first larval stage (Figure 13 a'').

## Chapter 4: DISCUSSION AND CONCLUSIONS

### 4.1 Model for cytoplasmic proteins to gain mechanistic insight into turnover

This study is an expansion of a study conducted by my lab in 2012 where it was discovered that mechanical force affects integrin turnover by changes in two rate constants:  $k_{\text{endo}}$ , which quantifies the rate of endocytic removal of integrins from the plasma membrane, and  $k_{\text{exo}}$ , which quantifies the rate of vesicle fusion leading to integrin delivery to the plasma membrane (Pines et al, 2012). Due to the fact that integrins are membrane receptors, Pines et al (2012) did not have to account for binding on and off the adhesions complex which, however, is necessary for cytoplasmic proteins. In this study, we have expanded the model (by Pines et al, 2012) for membrane proteins (integrin) to a more complicated model for cytoplasmic proteins (talin) characterised by four independent rate constants (as shown in Figure 7 and Figure 8).

This is the first study where four rate constants are derived to gain mechanistic insight into the turnover of cytoplasmic proteins in intact and live animals. The “double fitting” method (2.3.2) was developed for this project in collaboration with Alejandra Herrera (Dan Coombs’ lab, Department of Mathematics, UBC). This method allows us to distinguish between the two ways that contribute to the delivery of cytoplasmic proteins to the plasma membrane (characterized by  $k_{\text{on}}$  and  $k_{\text{asm}}$ ) and the two ways that contribute to protein removal from the plasma membrane (characterized by  $k_{\text{off}}$  and  $k_{\text{dis}}$ ).

The “double fitting” method takes advantage of the excellent protocol by Schulman et al. (2013) which describes a drug delivery method for early stages of *Drosophila* embryos. We utilise this method to deliver the endocytosis inhibitor dynasore into live embryos. This is followed by

mathematical modelling where a dynasore dataset is simultaneously fitted with its corresponding control where the embryos have not been treated with dynasore<sup>11</sup>. As it has been shown that endocytosis has a role in the disassembly of the adhesion complex (Ezratty et al., 2009), we fix all the rate constants except  $k_{\text{dis}}$  and assume that it is the only rate constant that differs between these two datasets. In this way, we are able to solve for all the four rate constants in the dataset of interest to gain mechanistic insight into protein turnover (further details on the double fitting method was described in 2.3.2).

The advantage of developing a four-parameter (i.e. four rate constants) model to describe the turnover of cytoplasmic proteins is that it gives much more detailed mechanistic insight into the protein turnover. If we would use the membrane model as outlined in Pines et al. (2012) for talin we would only get information about talin delivery to the plasma membrane i.e. we would be unable to determine whether it would be due to the assembly of the adhesion complex or due to talin binding to integrin that is already in the plasma membrane. However, the disadvantage of this new cytoplasmic model compared to our previously published membrane model is it requires two datasets for each experiment. Apart from the dataset of interest, a dataset of the corresponding genotype where the endocytosis has been inhibited (“dynasore dataset”) is required for the double fitting analysis that was discussed above. This makes the data collection for the cytoplasmic model more time-consuming than for the membrane model.

Lastly, the advantage of our experimental set-up is that it gives us information on how talin senses force in a whole-animal context. Most of the studies concerning mechnosensing at the

---

<sup>11</sup> See Appendix B for the dynasore datasets used in this study.

IAC have been performed *in vitro* or in cell culture systems. Our unique experimental set-up allows studying mechanosensing in an appropriate physiological context in living organisms.

## **4.2 Analysis of talin turnover in response to increased force**

### **4.2.1 Increased $k_{asm}$ is the main method of turnover regulation in response to increased force in WT talin**

My lab previously found out that increased force reduces the mobile fraction of WT talin (Pines et al., 2012) and was this observation confirmed in this study as can be seen in Figure 9 b'. Also, using our new cytoplasmic model, I found out that that increased force causes more assembly of talin to the plasma membrane since  $k_{asm}$  goes up significantly (+263% compared to -15% in the temperature control experiment (Figure 9 c)). This is consistent with our previous findings that less integrins are being removed from the plasma membrane when increased force acts on the MTJs (quantified by  $k_{endocytosis}$  in Figure 2b'' in Pines et al. (2012)). Thus, if increased force causes more integrins to be present at the plasma membrane it is logical that we see  $k_{asm}$  go up since there are more integrins participating in the complex assembly.

In WT talin,  $k_{dis}$  displays -44% reduction with increased force compared to -14% in the temperature control experiment (Figure 9 c). This suggests that the disassembly of the adhesion complex is significantly reduced under increased force. Furthermore,  $k_{off}$  displays +19% (and non-significant) relative change compared to +57% in the temperature control. In summary, increased force seems to cause more talin to be present at the plasma membrane as seen by increase in  $k_{asm}$  and decrease in  $k_{dis}$  and  $k_{off}$ . One explanation is that more talin is needed at the plasma membrane to form stronger and more stable adhesions to withstand the increased force.

#### **4.2.2 $k_{asm}$ becomes dysregulated in all of the talin mutants in response to increased force**

The mobile fraction analysis reveals that all of the talin mutants respond to increased force by a reduction in the mobile fraction as seen for WT talin (Figure 10 a'-e'). This indicates that the response to increased force is very robust.

The rate constant ratios reveal that in WT talin,  $k_{asm}/k_{dis}$  goes up by a factor of nearly 7 when increased force is acting on the MTJs. In contrast, in all of the talin mutants,  $k_{asm}/k_{dis}$  goes up by a factor of only roughly 1 to 2 (Figure 10 g). Furthermore, for all the talin mutants,  $k_{asm}$  shows a negative relative change as opposed to a great positive change as seen for WT talin (Figure 10 f). These findings indicate that in the talin mutants,  $k_{asm}$  becomes dysregulated under increased force.

In summary, none of the talin mutants that were tested were sufficient to completely abrogate talin's response to increased force as the overall mobile fraction reduces as seen for WT talin. Therefore, I suggest that there are overlapping mechanisms that ensure that the overall mobile fraction goes down even if a single domain within the talin molecule is mutated. However, mutated functional domains in talin can severely affect its response to force as seen by dysregulation in  $k_{asm}$  for all of the mutants. I speculate that this could lead to muscle detachment phenotypes because the adhesions do not build up at the plasma membrane as indicated by lower  $k_{asm}$  compared to WT. Therefore, there is a possibility that in the talin mutants the adhesions are not strong enough to withstand the increase in force.

### **4.2.3 $k_{on}$ becomes more dominant than $k_{off}$ in response to increased force for WT and talin mutants**

For WT talin in Brkd<sup>J29</sup> background, the relative changes in  $k_{on}$  and  $k_{off}$  display a very similar trend as seen for the temperature control (Figure 10 f). This indicates that the response to increased force is only slightly regulated through  $k_{off}$  and  $k_{on}$ . Despite this fact, when looking at the  $k_{on}/k_{off}$  ratio, it becomes clear that  $k_{on}$  is always more dominant than  $k_{off}$  at 37°C as compared to 25°C for WT and all of the talin mutants. This is seen by a lower  $k_{off}/k_{on}$  ratio at 37°C than 25°C (Figure 10 f). First, this indicates that increased force causes more talin to bind to the adhesion complex. Secondly, it seems that none of the talin mutants disrupt this process. One possible explanation is that the talin domains tested (i.e. talin mutants) are redundant to recruit talin to the plasma membrane under increased force by binding to the adhesion complex (as measured by  $k_{on}$ ).

### **4.2.4 $k_{on}$ and $k_{off}$ become dysregulated in the actin binding mutant in response to increased force**

The actin binding mutant shows the most different trend in regards to the relative changes from 25°C to 37°C in  $k_{on}$  and  $k_{off}$  compared to WT as both  $k_{on}$  and  $k_{off}$  display a negative change as opposed to positive change for WT (Figure 10 f). This suggests that talin binding ( $k_{on}$ ) and unbinding ( $k_{off}$ ) to the adhesion complex are disrupted when the actin binding domain is mutated.

It has been shown that the C-terminus part of the talin molecule<sup>12</sup>, “stretches as a spring” when the actomyosin contractile machine pulls on it when the N-terminus is linked to the plasma membrane and the C-terminus is bound to the actin cytoskeleton (via the actin binding/THATCH domain). Furthermore, it has been shown that stretching a single talin rod results in exposure of cryptic binding sites within the molecule (del Rio et al., 2009) (explained further in chapter 1.2.5). I propose that the reason why  $k_{on}$  and  $k_{off}$  become dysregulated under increased force in the actin binding mutant is because talin molecules are not “being stretched” as the binding to the actin cytoskeleton via the THATCH domain has been abrogated. Furthermore, the cryptic binding sites that would normally get exposed upon stretching could potentially affect talin binding ( $k_{on}$ ) and unbinding ( $k_{off}$ ) to the adhesion complex.

In summary, I speculate if the ability of talin to link to the actin cytoskeleton (via the THATCH domain) is abrogated, this phenomenon (i.e. stretching and exposure of cryptic binding sites) does not take place which could explain the dysregulation in  $k_{on}$  and  $k_{off}$  as seen for the actin binding mutant.

### **4.3 Analysis of talin turnover in response to decreased force**

#### **4.3.1 Decreased force does not affect the mobile fraction of WT talin**

The mobile fraction analysis reveals that decreased force does not affect the mobile fraction of WT talin (Figure 11 b<sup>1</sup>). In contrast, in a previous study from my lab, it was shown that decreased force increases the mobile fraction of the IAC components tensin and ILK (Pines et

---

<sup>12</sup> Often called the talin rod, see chapter 1.2.1 for further clarification.

al., 2012). I speculate that the reason why talin turnover stays the same under decreased force is because certain mechanisms ensure that talin turnover stays the same as talin is a core component of the IAC and works as a scaffold for multiple IAC components. In other words, I speculate that the reason why the mobile fraction of WT talin does not increase in response to decreased force (as seen for ILK and tensin as outlined in Pines et al. (2012)) is to prevent the IAC from undergoing too much disassociation because of the role of talin as a massive scaffold for other IAC components.

Interestingly, the rate constant analysis reveals effective increase in  $k_{on}$ ,  $k_{dis}$  and  $k_{asm}$  as they showed no significant change in response to elevated temperature while all these rate constants for WT showed significant change at elevated temperature. This suggests that decreased force changes the turnover kinetics without overall change in mobile fraction.

#### **4.3.2 Decreased force causes dysregulation in the turnover of talin that contains the IBS-2 mutant**

The IBS-2 mutant displays the most severe effects in turnover in response to decreased force for all of the talin mutants that were tested. The IBS-2 mutant is the only mutant that displays changes in the mobile fraction in response to decreased force (Figure 12 a'-e'). Moreover, the ratio  $k_{asm}/k_{dis}$  goes up by a factor of approximately 2 (11.4 to 23.1) compared to a slight increase (9.5 to 12.1) for WT (Figure 12 g). This indicates a disruption in the assembly of the adhesion complex.

My lab has previously shown that talin binding to integrin via the IBS-2 domain has a role in the assembly of the IAC. It was found out using immunohistochemistry that IAC markers (paxillin

and PINCH) do not colocalise with the  $\alpha$ PS2 integrin heterodimer when talin deficient embryos are rescued with talin containing the IBS-2 mutant. This indicates that the IBS-2 mutant makes the adhesions less stable (Ellis et al., 2011). This observation is consistent with my finding that the assembly of the adhesion complex is disrupted in larvae expressing talin that contains the IBS-2 mutant. Furthermore, the turnover of the IAC components has the tendency to increase when decreased force is acting on the MTJs (Pines et al., 2012). Therefore, I speculate that the IBS-2 mutant in a combination with decreased force could enhance turnover dysregulation. This could potentially explain why  $k_{on}$  and  $k_{off}$  display a great positive relative change compared to no significant change in  $k_{on}$  and a small negative relative change in  $k_{off}$  for WT (Figure 12 f). In conclusion, my data suggest that the IBS-2 domain in talin is required for turnover regulation when force is reduced.

### **4.3.3 Decreased force does not severely affect the turnover of WT talin, activation-, IBS-1-, and actin binding mutants**

The mobile fraction analysis shows that decreased force does not affect the mobile fraction of WT talin and any of the talin mutants except IBS-2 (Figure 12 a'-e'). This indicates that response to decreased force is fairly robust. This also suggests that there are multiple overlapping mechanisms that ensure that the overall mobile fraction stays the same even if a single domain is mutated.

The rate constant analysis reveals that  $k_{off}$  is the only rate constant that displays significant change in response to decreased force in WT talin (Figure 12 a''). In contrast,  $k_{off}$  becomes non-significant in response to decreased force for the activation mutant (Figure 12 b''). I propose that less talin mediated integrin activation is needed when decreased force is acting on the MTJs.

In particular, there might not be as much need to reinforce strong adhesions to the ECM under decreased force. Therefore, I speculate that in this particular situation, talin's ability to activate integrins and link them to the ECM is not as important as if the physiological forces were unchanged. This could partially explain why there are only subtle disruptions in the turnover of the activation mutant in response to decreased force (i.e. only  $k_{\text{off}}$  becomes non-significant).

As for the activation mutant, none of the rate constants for the actin binding mutant are affected by decreased force as opposed to only  $k_{\text{off}}$  for WT (compare Figure 12 a'' and e''). One potential explanation could be that linking talin to the actin cytoskeleton is not as important when decreased force is acting on the MTJs. Furthermore, for the same reason as mentioned in above paragraph, there might be less need for talin to reinforce the link between integrins and the cytoskeleton when force is decreased.

#### **4.4 Proposed model of integrin and talin turnover**

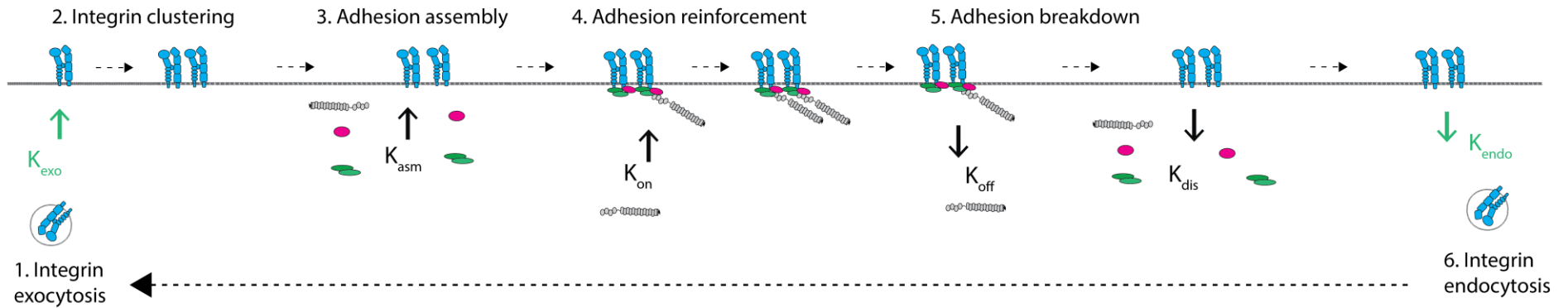
As mentioned earlier, my study is an expansion of a previous study conducted by my lab (Pines et al., 2012). Figure 14 summarizes and incorporates my results with the results from that previous study which was focused on analysing integrin turnover.

In the previous study, my lab found out that increased force causes increase in integrin exocytosis ( $k_{\text{exo}}$  in Figure 14 b). This fits well with my observation that talin delivery to the plasma membrane increases due to the increased assembly of the adhesion complex ( $k_{\text{asm}}$  in Figure 14 b) as there are more integrin present at the plasma membrane to participate in the assembly of the adhesion complex. In addition, increased force does not seem to affect talin binding to and from the adhesion complex ( $k_{\text{on}}$  and  $k_{\text{off}}$  in Figure 14 b). Furthermore, in the

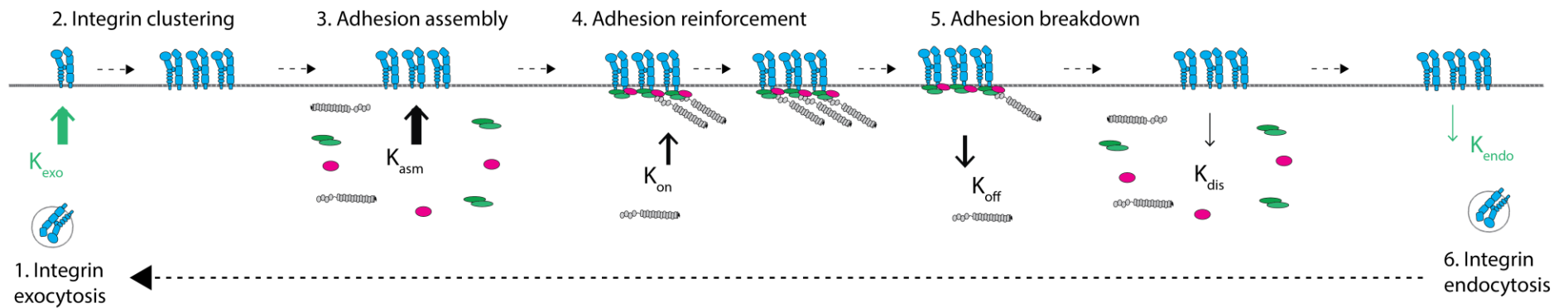
previous study it was found out that increased force causes reduction in integrin endocytosis ( $k_{\text{endo}}$  in Figure 14 b). This also fits with my observation that talin removal from the plasma membrane due to the disassembly of the adhesion complex ( $k_{\text{dis}}$  in Figure 14 b) is reduced with increased force as there is less breakdowns of the adhesions. I speculate that increased force causes the adhesions to become stronger and more stable by regulation through all of the rate constants mentioned above except  $k_{\text{on}}$  and  $k_{\text{off}}$ .

Decreased force seems to have more subtle effect on the turnover of WT talin and integrin than increased force. In the previous study (Pines et al., 2012), it was found out that decreased force slightly increases integrin exocytosis and endocytosis ( $k_{\text{exo}}$  and  $k_{\text{endo}}$  in Figure 14 c). This is consistent with my observation that decreased force slightly increases all of the rate constants ( $k_{\text{exo}}$ ,  $k_{\text{endo}}$ ,  $k_{\text{on}}$  and  $k_{\text{off}}$  in Figure 14 c) as compared to WT because there are more integrins at the plasma membrane to assemble the complex. However, this increase is in most cases very subtle and the effects are not as pronounced as seen for increased force. Furthermore, decreased force does not affect the overall mobile fraction. Therefore, I speculate that decreased force enhances talin turnover but there are mechanisms in place to ensure that the overall mobile fraction stays the same.

**(a) Control (WT)**



**(b) Increased force (*Brkd*<sup>J29</sup>)**



**(c) Decreased force (*para*<sup>ts2</sup>)**

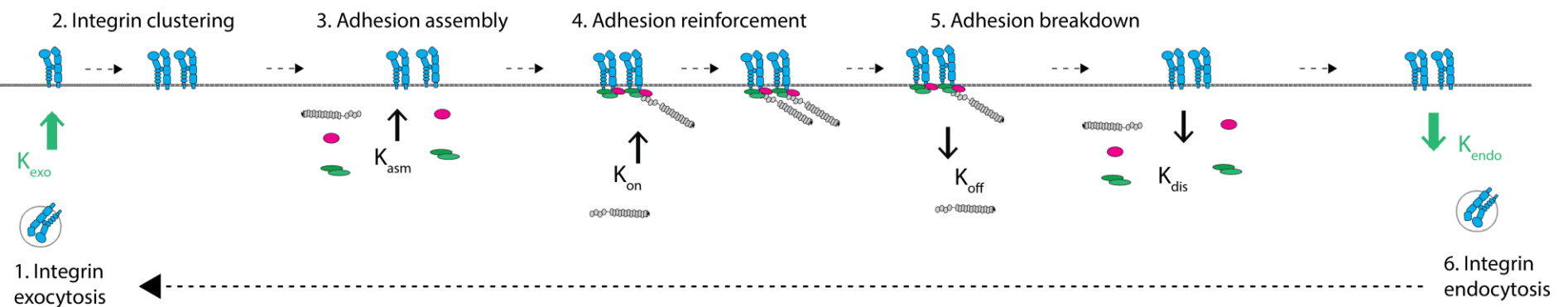


**Figure 14: Proposed model of turnover for WT integrin and talin in response to altered force.**

**Figure 14: Proposed model of turnover for WT integrin and talin in response to altered force.** Rate constants in green are for integrins, see Pines et al. (2012). Rate constants in black are for talin (this study). Rate constants in equilibrium are denoted by medium thick arrows. Increase in rate constants are denoted by thick arrows and decrease in rate constants are denoted by thin arrows.

(A) Control i.e. talin in WT background. The rate constants are in equilibrium.

(B) Increased force i.e. talin in Brkd<sup>J29</sup> background. There is a dramatic increase in  $k_{\text{exo}}$  and  $k_{\text{asm}}$  as donated by three integrin molecules at the plasma membrane (as opposed to two integrin molecules for scenarios A and C).

(C) Decreased force i.e. talin in para<sup>ts2</sup> background.

**Step 1: integrin exocytosis** - Integrins are delivered to the plasma membrane by vesicle fusion (measured by  $k_{\text{exo}}$ ).

**Step 2: integrin clustering** - Integrins cluster at the plasma membrane.

**Step 3: adhesion assembly** - The IAC (including talin) assembles around the integrin cytoplasmic tail (measured by  $k_{\text{asm}}$ ).

**Step 4: adhesion reinforcement** – talin binds to the IAC to reinforce adhesions (measured by  $k_{\text{on}}$ ).

**Step 5: adhesion breakdown** – adhesions undergo breakdown as talin unbinds the IAC (measured by  $k_{\text{off}}$ ) and subsequently the IAC undergoes disassembly (measured by  $k_{\text{dis}}$ ).

**Step 6: integrin endocytosis** – integrins are endocytosed into the cytoplasm where they can be exocytosed again (see Step 1).

#### **4.5 During *Drosophila* embryogenesis and larval development there are two mechanisms that regulate talin turnover**

My lab has previously shown that during *Drosophila* larval stages, the muscles undergo dramatic growth and increase in the MTJ width (Yuan et al., 2010). Furthermore, by the end of embryogenesis (end of embryonic stage 17) the animal becomes more mobile as the larva begins to crawl. These results indicate that more force acts on the MTJs in larvae compared to embryos.

My data suggest that there is a different mechanism in place during embryogenesis and larval development to ensure the MTJs stability in response to force (see Figure 13).  $K_{on}$  for the embryonic stages is substantially lower than in the larval stage which suggests that more talin is binding to the IAC at the plasma membrane. I speculate that this is part of a mechanism that ensures stronger adhesions to withstand the increases in force as the animal grows. In contrast,  $k_{off}$  displays the highest value for embryonic stage 16. This suggests that there is more talin unbinding integrin at the plasma membrane when relative low force is acting on the MTJs. One explanation could be that this is a part of mechanisms that allows MTJs remodelling and growth as development progresses. Furthermore,  $k_{dis}$  shows a stage-dependant decrease. This suggests that there is less disassembly of the adhesion complex as development progresses. In contrast,  $k_{asm}$  displays the highest value for L3 suggesting more assembly of the adhesion complex than in earlier developmental stages.

In conclusion, these results indicate that there is an early mechanism that allows the remodelling of the adhesions during embryogenesis. Secondly, there is a late mechanism that ensures that the adhesions are strong and stable to withstand the increase in force in larval development.

## 4.6 Conclusions

I confirmed my hypothesis (as outlined in 1.5.2) that certain functional domains within talin are required for sensing force at the MTJs in *Drosophila* larvae and embryos. In particular, I found out that various mutants in the functional domains of the talin molecule either abrogate or severely affect talin's ability to respond to force.

In most cases where talin mutants affect talin's ability to respond to force, the mobile fraction has the same trend as WT but some or all of the rate constants display significant differences compared to WT. This scenario is true for all of the talin mutants that were tested in response to increased force. This suggests that there are overlapping mechanisms that ensure that the mobile fraction stays the same even if an individual domain is mutated but the response to force is severely affected as revealed by changes in the rate constants. Furthermore, this demonstrates that all of the talin mutants respond to increased force but they do it a lot less effectively compared to WT. Lastly, the fact that I did not find any talin mutants that completely abrogated talin's response to increased force indicates that the response is very robust. Further research might investigate whether making a double mutant/s would completely abrogate talin's response to increased force. However, since most of the mutants used in this study are in domains that localize talin to the adhesions, using a double mutant could severely disrupt talin localization to the adhesions which could complicate our FRAP assays.

Regarding talin turnover in response to decreased force, I found out that the IBS-2 mutant almost completely abrogates the response. First, this is demonstrated by significant reduction in the mobile fraction compared to WT. Secondly, there is a dramatic increase in the rate constants

compared to WT. This suggests that the IBS-2 domain in talin is required for turnover in response to decreased force.

Furthermore, my results for the turnover of WT talin are consistent with previous study (Pines et al., 2012) from my lab that focused on analysing the turnover of integrin. To highlight the consistency between these two studies, I made a schematic of a speculative model that describes integrin and talin turnover in response to altered force (Figure 14). The main conclusions from this model are: 1) the adhesions become stronger and more stable when increased force acts on the MTJs and, 2) decreased force has subtle effect on the adhesions as it enhances the turnover without affecting the mobile fraction of talin.

Finally, I confirmed previous results from my lab (Yuan et al., 2010) that the turnover of WT talin is developmentally regulated. In addition, the rate constant analysis reveals that this regulation is due to two mechanisms: an early mechanism that takes place in embryogenesis and, a late mechanism that takes place in larval development.

## Bibliography

- Alatortsev, V.E., I.A. Kramerova, M.V. Frolov, S.A. Lavrov, and E.D. Westphal. 1997. Vinculin gene is non-essential in *Drosophila melanogaster*. *FEBS letters*. 413:197-201.
- Anthis, N.J., K.L. Wegener, F. Ye, C. Kim, B.T. Goult, E.D. Lowe, I. Vakonakis, N. Bate, D.R. Critchley, M.H. Ginsberg, and I.D. Campbell. 2009. The structure of an integrin/talin complex reveals the basis of inside-out signal transduction. *The EMBO journal*. 28:3623-3632.
- Askari, J.A., P.A. Buckley, A.P. Mould, and M.J. Humphries. 2009. Linking integrin conformation to function. *J Cell Sci*. 122:165-170.
- Ballestrem, C., B. Hinz, B.A. Imhof, and B. Wehrle-Haller. 2001. Marching at the front and dragging behind: differential  $\alpha\text{V}\beta\text{3}$ -integrin turnover regulates focal adhesion behavior. *The Journal of Cell Biology*. 155:1319-1332.
- Bos, J.L. 2005. Linking Rap to cell adhesion. *Current Opinion in Cell Biology*. 17:123-128.
- Bretscher, M.S. 1989. Endocytosis and recycling of the fibronectin receptor in CHO cells. *The EMBO journal*. 8:1341-1348.
- Bretscher, M.S. 1992. Circulating integrins: alpha 5 beta 1, alpha 6 beta 4 and Mac-1, but not alpha 3 beta 1, alpha 4 beta 1 or LFA-1. *The EMBO journal*. 11:405-410.
- Bridgewater, R.E., J.C. Norman, and P.T. Caswell. 2012. Integrin trafficking at a glance. *J Cell Sci*. 125:3695-3701.
- Brower, D.L., M. Wilcox, M. Piovant, R.J. Smith, and L.A. Reger. 1984. Related cell-surface antigens expressed with positional specificity in *Drosophila* imaginal discs. *Proceedings of the National Academy of Sciences of the United States of America*. 81:7485-7489.
- Brown, N.H., S.L. Gregory, and Z.D. Martin-Bermudo. 2000. Integrins as mediators of morphogenesis in *Drosophila*. *Developmental Biology*. 223:1-16.
- Brown, N.H., S.L. Gregory, W.L. Rickoll, L.I. Fessler, M. Prout, R.A. White, and J.W. Fristrom. 2002. Talin is essential for integrin function in *Drosophila*. *Developmental cell*. 3:569-579.
- Bulgakova, N.A., B. Klapholz, and N.H. Brown. 2012. Cell adhesion in *Drosophila*: versatility of cadherin and integrin complexes during development. *Current Opinion in Cell Biology*. 24:702-712.
- Burridge, K., and L. Connell. 1983. A new protein of adhesion plaques and ruffling membranes. *J Cell Biol*. 97:359-367.
- Calderwood, D.A., B. Yan, J.M. de Pereda, B.G.a. Alvarez, Y. Fujioka, R.C. Liddington, and M.H. Ginsberg. 2002. The Phosphotyrosine Binding-like Domain of Talin Activates Integrins. *Journal of Biological Chemistry*. 277:21749-21758.
- Calderwood, D.A., R. Zent, R. Grant, D.J. Rees, R.O. Hynes, and M.H. Ginsberg. 1999. The Talin head domain binds to integrin beta subunit cytoplasmic tails and regulates integrin activation. *The Journal of biological chemistry*. 274:28071-28074.
- Caswell, P.T., and J.C. Norman. 2006. Integrin trafficking and the control of cell migration. *Traffic (Copenhagen, Denmark)*. 7:14-21.
- Caswell, P.T., J.C. Norman, and S. Vadrevu. 2009. Integrins: masters and slaves of endocytic transport. *Nature Reviews Molecular Cell Biology*. 10:843+.

- Clark, K.A., M. McGrail, and M.C. Beckerle. 2003. Analysis of PINCH function in *Drosophila* demonstrates its requirement in integrin-dependent cellular processes. *Development*. 130:2611-2621.
- Critchley, D.R., and A.R. Gingras. 2008. Talin at a glance. *J Cell Sci*. 121:1345-1347.
- De Deyne, P.G., A. O'Neill, W.G. Resneck, G.M. Dmytrenko, D.W. Pumphlin, and R.J. Bloch. 1998. The vitronectin receptor associates with clathrin-coated membrane domains via the cytoplasmic domain of its beta5 subunit. *J Cell Sci*. 111 ( Pt 18):2729-2740.
- del Rio, A., R. Perez-Jimenez, R. Liu, P. Roca-Cusachs, J.M. Fernandez, and M.P. Sheetz. 2009. Stretching single talin rod molecules activates vinculin binding. *Science (New York, N.Y.)*. 323:638-641.
- Desgrosellier, J.S., and D.A. Cheresh. 2010. Integrins in cancer: biological implications and therapeutic opportunities. *Nat Rev Cancer*. 10:9-22.
- Dumbauld, D.W., T.T. Lee, A. Singh, J. Scrimgeour, C.A. Gersbach, E.A. Zamir, J. Fu, C.S. Chen, J.E. Curtis, S.W. Craig, and A.J. García. 2013. How vinculin regulates force transmission. *Proceedings of the National Academy of Sciences*. 110:9788-9793.
- Ellis, S.J., E. Lostchuck, B.T. Goult, M. Bouaouina, M.J. Fairchild, P. Lopez-Ceballos, D.A. Calderwood, and G. Tanentzapf. 2014. The talin head domain reinforces integrin-mediated adhesion by promoting adhesion complex stability and clustering. *PLoS genetics*. 10:e1004756.
- Ellis, S.J., M. Pines, M.J. Fairchild, and G. Tanentzapf. 2011. In vivo functional analysis reveals specific roles for the integrin-binding sites of talin. *Journal of Cell Science*. 124:1844-1856.
- Ezratty, E.J., C. Bertaux, E.E. Marcantonio, and G.G. Gundersen. 2009. Clathrin mediates integrin endocytosis for focal adhesion disassembly in migrating cells. *The Journal of Cell Biology*. 187:733-747.
- Ezratty, E.J., M.A. Partridge, and G.G. Gundersen. 2005. Microtubule-induced focal adhesion disassembly is mediated by dynamin and focal adhesion kinase. *Nat Cell Biol*. 7:581-590.
- Franco-Cea, A., S.J. Ellis, M.J. Fairchild, L. Yuan, T.Y. Cheung, and G. Tanentzapf. 2010. Distinct developmental roles for direct and indirect talin-mediated linkage to actin. *Dev Biol*. 345:64-77.
- Friedland, J.C., M.H. Lee, and D. Boettiger. 2009. Mechanically activated integrin switch controls alpha5beta1 function. *Science (New York, N.Y.)*. 323:642-644.
- Galbraith, C.G., K.M. Yamada, and M.P. Sheetz. 2002. The relationship between force and focal complex development. *J Cell Biol*. 159:695-705.
- García-Alvarez, B., J.M. de Pereda, D.A. Calderwood, T.S. Ulmer, D. Critchley, I.D. Campbell, M.H. Ginsberg, and R.C. Liddington. 2003. Structural Determinants of Integrin Recognition by Talin. *Molecular Cell*. 11:49-58.
- Geiger, B., J.P. Spatz, and A.D. Bershadsky. 2009. Environmental sensing through focal adhesions. *Nature reviews. Molecular cell biology*. 10:21-33.
- Gingras, A.R., N. Bate, B.T. Goult, L. Hazelwood, I. Canestrelli, J.G. Grossmann, H. Liu, N.S.M. Putz, G.C.K. Roberts, N. Volkmann, D. Hanein, I.L. Barsukov, and D.R. Critchley. 2008. The structure of the C-terminal actin-binding domain of talin. *The EMBO journal*. 27:458-469.
- Gingras, A.R., W.H. Ziegler, A.A. Bobkov, M.G. Joyce, D. Fasci, M. Himmel, S. Rothmund, A. Ritter, J.G. Grossmann, B. Patel, N. Bate, B.T. Goult, J. Emsley, I.L. Barsukov, G.C. Roberts, R.C. Liddington, M.H. Ginsberg, and D.R. Critchley. 2009. Structural

- determinants of integrin binding to the talin rod. *The Journal of biological chemistry*. 284:8866-8876.
- Goksoy, E., Y.-Q. Ma, X. Wang, X. Kong, D. Perera, E.F. Plow, and J. Qin. 2008. Structural Basis for the Autoinhibition of Talin in Regulating Integrin Activation. *Molecular Cell*. 31:124-133.
- Goldmann, W.H., A. Bremer, M. Haner, U. Aebi, and G. Isenberg. 1994. Native talin is a dumbbell-shaped homodimer when it interacts with actin. *Journal of structural biology*. 112:3-10.
- Goult, B.T., N. Bate, N.J. Anthis, K.L. Wegener, A.R. Gingras, B. Patel, I.L. Barsukov, I.D. Campbell, G.C.K. Roberts, and D.R. Critchley. 2009. The Structure of an Interdomain Complex That Regulates Talin Activity. *Journal of Biological Chemistry*. 284:15097-15106.
- Goult, B.T., T. Zacharchenko, N. Bate, R. Tsang, F. Hey, A.R. Gingras, P.R. Elliott, G.C. Roberts, C. Ballestrem, D.R. Critchley, and I.L. Barsukov. 2013. RIAM and vinculin binding to talin are mutually exclusive and regulate adhesion assembly and turnover. *The Journal of biological chemistry*. 288:8238-8249.
- Grabbe, C., C.G. Zervas, T. Hunter, N.H. Brown, and R.H. Palmer. 2004. Focal adhesion kinase is not required for integrin function or viability in *Drosophila*. *Development*. 131:5795-5805.
- Grigliatti, T., D.T. Suzuki, and R. Williamson. 1972. Temperature-sensitive mutation in *Drosophila melanogaster*. X. Developmental analysis of the paralytic mutation, para ts. *Dev Biol*. 28:352-371.
- Haling, J.R., S.J. Monkley, D.R. Critchley, and B.G. Petrich. 2011. Talin-dependent integrin activation is required for fibrin clot retraction by platelets. *Blood*. 117:1719-1722.
- Harburger, D.S., M. Bouaouina, and D.A. Calderwood. 2009. Kindlin-1 and -2 Directly Bind the C-terminal Region of  $\beta$  Integrin Cytoplasmic Tails and Exert Integrin-specific Activation Effects. *Journal of Biological Chemistry*. 284:11485-11497.
- Horwitz, A., K. Duggan, C. Buck, M.C. Beckerle, and K. Burridge. 1986. Interaction of plasma membrane fibronectin receptor with talin—a transmembrane linkage. *Nature*. 320:531-533.
- Humphries, J.D., A. Byron, and M.J. Humphries. 2006. Integrin ligands at a glance. *J Cell Sci*. 119:3901-3903.
- Hynes, R.O. 1987. Integrins: A family of cell surface receptors. *Cell*. 48:549-554.
- Hynes, R.O. 2002. Integrins: Bidirectional, Allosteric Signaling Machines. *Cell*. 110:673-687.
- Jiang, G., G. Giannone, D.R. Critchley, E. Fukumoto, and M.P. Sheetz. 2003. Two-piconewton slip bond between fibronectin and the cytoskeleton depends on talin. *Nature*. 424:334-337.
- Kong, F., A.J. Garcia, A.P. Mould, M.J. Humphries, and C. Zhu. 2009. Demonstration of catch bonds between an integrin and its ligand. *J Cell Biol*. 185:1275-1284.
- Kopp, P.M., N. Bate, T.M. Hansen, N.P.J. Brindle, U. Praekelt, E. Debrand, S. Coleman, D. Mazzeo, B.T. Goult, A.R. Gingras, C.A. Pritchard, D.R. Critchley, and S.J. Monkley. 2010. Studies on the morphology and spreading of human endothelial cells define key inter- and intramolecular interactions for talin1. *European Journal of Cell Biology*. 89:661-673.

- Lavelin, I., H. Wolfenson, I. Patla, Y.I. Henis, O. Medalia, T. Volberg, A. Livne, Z. Kam, and B. Geiger. 2013. Differential Effect of Actomyosin Relaxation on the Dynamic Properties of Focal Adhesion Proteins. *PloS one*. 8:1-1.
- Lee, H.S., P. Anekal, C.J. Lim, C.C. Liu, and M.H. Ginsberg. 2013. Two modes of integrin activation form a binary molecular switch in adhesion maturation. *Molecular biology of the cell*. 24:1354-1362.
- Lee, H.S., C.J. Lim, W. Puzon-McLaughlin, S.J. Shattil, and M.H. Ginsberg. 2009. RIAM activates integrins by linking talin to ras GTPase membrane-targeting sequences. *The Journal of biological chemistry*. 284:5119-5127.
- Liu, S., D.A. Calderwood, and M.H. Ginsberg. 2000. Integrin cytoplasmic domain-binding proteins. *Journal of Cell Science*. 113:3563-3571.
- Macia, E., M. Ehrlich, R. Massol, E. Boucrot, C. Brunner, and T. Kirchhausen. 2006. Dynasore, a Cell-Permeable Inhibitor of Dynamin. *Developmental cell*. 10:839-850.
- Martel, V., L. Vignoud, S. Dupe, P. Frchet, M.R. Block, and C. Albiges-Rizo. 2000. Talin controls the exit of the integrin alpha 5 beta 1 from an early compartment of the secretory pathway. *J Cell Sci*. 113 ( Pt 11):1951-1961.
- McCabe, N.P., S. De, A. VasANJI, J. Brainard, and T.V. Byzova. 2007. Prostate cancer specific integrin  $\alpha\beta 3$  modulates bone metastatic growth and tissue remodeling. *Oncogene*. 26:6238-6243.
- McCann, R.O., and S.W. Craig. 1999. Functional Genomic Analysis Reveals the Utility of the I/LWEQ Module as a Predictor of Protein:Actin Interaction. *Biochemical and Biophysical Research Communications*. 266:135-140.
- Moes, M., S. Rodius, S.J. Coleman, S.J. Monkley, E. Goormaghtigh, L. Tremuth, C. Kox, P.P. van der Holst, D.R. Critchley, and N. Kieffer. 2007. The integrin binding site 2 (IBS2) in the talin rod domain is essential for linking integrin beta subunits to the cytoskeleton. *The Journal of biological chemistry*. 282:17280-17288.
- Montana, E.S., and J.T. Littleton. 2004. Characterization of a hypercontraction-induced myopathy in *Drosophila* caused by mutations in Mhc. *The Journal of Cell Biology*. 164:1045-1054.
- Ni, H., and J. Freedman. 2003. Platelets in hemostasis and thrombosis: role of integrins and their ligands. *Transfusion and apheresis science : official journal of the World Apheresis Association : official journal of the European Society for Haemapheresis*. 28:257-264.
- Parsons, J.T., A.R. Horwitz, and M.A. Schwartz. 2010. Cell adhesion: integrating cytoskeletal dynamics and cellular tension. *Nature reviews. Molecular cell biology*. 11:633-643.
- Pellinen, T., A. Arjonen, K. Vuoriluoto, K. Kallio, J.A. Fransen, and J. Ivaska. 2006. Small GTPase Rab21 regulates cell adhesion and controls endosomal traffic of beta1-integrins. *J Cell Biol*. 173:767-780.
- Pines, M., R. Das, S.J. Ellis, A. Morin, S. Czerniecki, L. Yuan, M. Klose, D. Coombs, and G. Tanentzapf. 2012. Mechanical force regulates integrin turnover in *Drosophila* in vivo. *Nat. Cell Biol*. 14:935-+.
- Pittendrigh, B., R. Reenan, R.H. French-Constant, and B. Ganetzky. 1997. Point mutations in the *Drosophila* sodium channel gene para associated with resistance to DDT and pyrethroid insecticides. *Mol Gen Genet*. 256:602-610.
- Prokop, A., M.D. Martín-Bermudo, M. Bate, and N.H. Brown. 1998. Absence of PS Integrins or Laminin A Affects Extracellular Adhesion, but Not Intracellular Assembly, of

- Hemidherens and Neuromuscular Junctions in *Drosophila* Embryos. *Developmental Biology*. 196:58-76.
- Prout, M., Z. Damania, J. Soong, D. Fristrom, and J.W. Fristrom. 1997. Autosomal mutations affecting adhesion between wing surfaces in *Drosophila melanogaster*. *Genetics*. 146:275-285.
- Puklin-Faucher, E., M. Gao, K. Schulten, and V. Vogel. 2006. How the headpiece hinge angle is opened: New insights into the dynamics of integrin activation. *J Cell Biol*. 175:349-360.
- Ramsay, A.G., M.D. Keppler, M. Jazayeri, G.J. Thomas, M. Parsons, S. Violette, P. Weinreb, I.R. Hart, and J.F. Marshall. 2007. HS1-associated protein X-1 regulates carcinoma cell migration and invasion via clathrin-mediated endocytosis of integrin  $\alpha$ v $\beta$ 6. *Cancer research*. 67:5275-5284.
- Reits, E.A.J., and J.J. Neefjes. 2001. From fixed to FRAP: measuring protein mobility and activity in living cells. *Nat Cell Biol*. 3:E145-E147.
- Rodius, S., O. Chaloin, M. Moes, E. Schaffner-Reckinger, I. Landrieu, G. Lippens, M. Lin, J. Zhang, and N. Kieffer. 2008. The talin rod IBS2  $\alpha$ -helix interacts with the  $\beta$ 3 integrin cytoplasmic tail membrane-proximal helix by establishing charge complementary salt bridges. *The Journal of biological chemistry*. 283:24212-24223.
- Sanyal, S., A. Basole, and K.S. Krishnan. 1999. Phenotypic Interaction between Temperature-Sensitive Paralytic Mutants comatose and paralytic Suggests a Role for N-Ethylmaleimide-Sensitive Fusion Factor in Synaptic Vesicle Cycling in *Drosophila*. *The Journal of Neuroscience*. 19:RC47.
- Sawada, Y., M. Tamada, B.J. Dubin-Thaler, O. Cherniavskaya, R. Sakai, S. Tanaka, and M.P. Sheetz. 2006. Force sensing by mechanical extension of the Src family kinase substrate p130Cas. *Cell*. 127:1015-1026.
- Schiller, H.B., and R. Fassler. 2013. Mechanosensitivity and compositional dynamics of cell-matrix adhesions. *EMBO Rep*. 14:509-519.
- Schiller, H.B., C.C. Friedel, C. Boulegue, and R. Fassler. 2011. Quantitative proteomics of the integrin adhesome show a myosin II-dependent recruitment of LIM domain proteins. *EMBO Rep*. 12:259-266.
- Schulman, V.K., E.S. Folker, and M.K. Baylies. 2013. A method for reversible drug delivery to internal tissues of *Drosophila* embryos. *Fly*. 7:193-203.
- Shi, F., and J. Sottile. 2008. Caveolin-1-dependent  $\beta$ 1 integrin endocytosis is a critical regulator of fibronectin turnover. *J Cell Sci*. 121:2360-2371.
- Smith, S.J., and R.O. McCann. 2007. A C-terminal dimerization motif is required for focal adhesion targeting of Talin1 and the interaction of the Talin1 I/LWEQ module with F-actin. *Biochemistry*. 46:10886-10898.
- Stenmark, H. 2009. Rab GTPases as coordinators of vesicle traffic. *Nature reviews. Molecular cell biology*. 10:513-525.
- Tanentzapf, G., and N.H. Brown. 2006. An interaction between integrin and the talin FERM domain mediates integrin activation but not linkage to the cytoskeleton. *Nat Cell Biol*. 8:601-606.
- Tanentzapf, G., M.D. Martin-Bermudo, M.S. Hicks, and N.H. Brown. 2006. Multiple factors contribute to integrin-talin interactions in vivo. *J Cell Sci*. 119:1632-1644.
- Tempel, M., W.H. Goldmann, G. Isenberg, and E. Sackmann. 1995. Interaction of the 47-kDa talin fragment and the 32-kDa vinculin fragment with acidic phospholipids: a computer analysis. *Biophysical Journal*. 69:228-241.

- Tepass, U. 2009. FERM proteins in animal morphogenesis. *Current opinion in genetics & development*. 19:357-367.
- Torgler, C.N., M. Narasimha, A.L. Knox, C.G. Zervas, M.C. Vernon, and N.H. Brown. 2004. Tensin stabilizes integrin adhesive contacts in *Drosophila*. *Developmental cell*. 6:357-369.
- Upla, P., V. Marjomaki, P. Kankaanpaa, J. Ivaska, T. Hyypia, F.G. Van Der Goot, and J. Heino. 2004. Clustering induces a lateral redistribution of alpha 2 beta 1 integrin from membrane rafts to caveolae and subsequent protein kinase C-dependent internalization. *Molecular biology of the cell*. 15:625-636.
- Wegener, K.L., A.W. Partridge, J. Han, A.R. Pickford, R.C. Liddington, M.H. Ginsberg, and I.D. Campbell. 2007. Structural basis of integrin activation by talin. *Cell*. 128:171-182.
- Wolfenson, H., A. Bershadsky, Y.I. Henis, and B. Geiger. 2011. Actomyosin-generated tension controls the molecular kinetics of focal adhesions. *J Cell Sci*. 124:1425-1432.
- Wolfenson, H., I. Lavelin, and B. Geiger. 2013. Dynamic regulation of the structure and functions of integrin adhesions. *Developmental cell*. 24:447-458.
- Wolfenson, H., A. Lubelski, T. Regev, J. Klafter, Y.I. Henis, and B. Geiger. 2009. A role for the juxtamembrane cytoplasm in the molecular dynamics of focal adhesions. *PLoS one*. 4:e4304.
- Yagi, R., S. Ishimaru, H. Yano, U. Gaul, H. Hanafusa, and H. Sabe. 2001. A novel muscle LIM-only protein is generated from the paxillin gene locus in *Drosophila*. *EMBO Reports*. 2:814-820.
- Yao, M., B.T. Goult, H. Chen, P. Cong, M.P. Sheetz, and J. Yan. 2014. Mechanical activation of vinculin binding to talin locks talin in an unfolded conformation. *Sci. Rep.* 4.
- Ye, F., G. Hu, D. Taylor, B. Ratnikov, A.A. Bobkov, M.A. McLean, S.G. Sligar, K.A. Taylor, and M.H. Ginsberg. 2010. Recreation of the terminal events in physiological integrin activation. *J Cell Biol.* 188:157-173.
- Yoshigi, M., L.M. Hoffman, C.C. Jensen, H.J. Yost, and M.C. Beckerle. 2005. Mechanical force mobilizes zyxin from focal adhesions to actin filaments and regulates cytoskeletal reinforcement. *The Journal of Cell Biology*. 171:209-215.
- Yuan, L., M.J. Fairchild, A.D. Perkins, and G. Tanentzapf. 2010. Analysis of integrin turnover in fly myotendinous junctions. *Journal of Cell Science*. 123:939-946.
- Zaidel-Bar, R., and B. Geiger. 2010. The switchable integrin adhesome. *Journal of Cell Science*. 123:1385-1388.
- Zervas, C.G., S.L. Gregory, and N.H. Brown. 2001. *Drosophila* integrin-linked kinase is required at sites of integrin adhesion to link the cytoskeleton to the plasma membrane. *J Cell Biol.* 152:1007-1018.
- Ziegler, W.H., A.R. Gingras, D.R. Critchley, and J. Emsley. 2008. Integrin connections to the cytoskeleton through talin and vinculin. *Biochemical Society transactions*. 36:235-239.

## Appendices

### Appendix A - Mathematical analysis of FRAP data (author: Alejandra Herrera, 2015)

[This is a modified of version of Alejandra Herrera's thesis proposal draft and is used with the author's permission]

Talin will be fluorescently labeled and the FRAP curve represents the dynamics of the concentration of IAC at the plasma membrane. We neglect the possibility when some talin proteins are close to the plasma membrane but not bound to integrins. We will consider talin independent from integrins.

We will assume the observed fluorescence comes from two basic mechanisms. One will be given by the binding of talin (P) to Integrin (I) in the plasma membrane to form the bound complex I-P. We require integrins to be at the plasma membrane. The binding could be part or not of a full IAC. The second way is by the assembly of the IAC (C) inside the cell and its externalization to the plasma membrane. Here, integrins are assumed to be inside the cell (e.g. vesicles). In this case, we will consider all the cases where talin binding to integrins did not happen at the plasma membrane. The I-P binding could occur during the internalization pathway, as a cytosolic binding, or an instantaneous formation of the whole complex right before recycling of integrins happen. For the second case, we also count those not fully formed complexes where I-P binding somehow happens inside the cell (Martel et al., 2000; Tanentzapf et al., 2006). Then the observed FRAP data correspond to the I-P bound at the plasma membrane and the complex at the plasma membrane (C).

Then we have a compartmental model consisting of: free and fluorescently labeled cytosolic proteins talin (P), membrane protein integrin ( $I_m$ ), the integrin adhesion complex or I-P binding complex, both at the plasma membrane ( $C_m$ ), and I-P binding complex and other components of the complex that are not at the plasma membrane ( $C_d$ ). To simplify the notation we will call "binding/unbinding" only when integrin is at the plasma membrane and talin binds to it, and we will call "assemble/disassemble" when the integrin and talin binding happens internally and possible the complex is formed during externalization. We assume that integrins at the plasma membrane will bind/unbind talin at rates  $k_{on}$  and  $k_{off}$  respectively. We also assume that integrin and talin will assemble the IAC from the cytosol at rate  $k_{asm}$  and the complex is disassembled and integrins undergo internalization at rate  $k_{dis}$ .

We consider that the natural photo-bleaching of the fluorescence protein occurs only when talin is bound to integrin in the plasma membrane and not in cytosolic proteins, since the external stimuli only affect the plasma membrane components. Prior to photo-bleaching, the system is assumed to be at chemical equilibrium and the natural photo-bleaching rate to be  $\delta=0$ . Assuming that the FRAP experiment does not disrupt the chemical equilibrium, the integrin concentration  $I_m$  remains at this pre-bleaching equilibrium during the recovery phase. In which case, we treat it as constant  $\hat{I}_m$ .



where  $k_{on} = k_{on} \hat{I}_m$ , with initial conditions

$$m(0) = \begin{cases} 0 & \text{recovery region} \\ 1 & \text{reference region} \end{cases}, \quad p(0) = \frac{P_{eq}}{(C_m)_{eq}} = \frac{k_{off}}{k_{on}}, \quad c(0) = \frac{(C_d)_{eq}}{(C_m)_{eq}} = \frac{k_{dis}}{k_{asm}}$$

This is a linear system of ODE that can be solved analytically. In this case,  $m$  corresponds to the normalized recovery data and we cannot use the FRAP data to measure either  $p$  or  $c$ . To find the best estimates of the parameters, we solve the system numerically and minimize the sum of square residuals (SSR) between the solution of  $m$  and the data. In other words, all our estimates depend only on  $m$ . The missing information about the cytosolic variables  $p$  and  $v$  creates an inherent symmetry in the system. If we exchange  $k_{dis} < > k_{off}$  and  $k_{asm} < > k_{on}$  we will end up with basically the same equation for  $m$  but with opposite interpretation for  $p$  and  $c$ . Therefore we will have two sets of parameters with the same SSR but with symmetric interpretation.

In order to numerically differentiate the disassemble from the disassociation rate and the assemble from the binding rates, we experimentally use an endocytosis inhibitor called dynasore (DYN). Endocytosis is necessary for disassemble of the IAC, and then we assume that by inhibiting endocytosis we are only affecting the disassembly process. Dynasore is believed to affect only the endocytosis of integrin vesicles, changing their recycling from the plasma membrane. We assumed that dynasore does not affect any other aspects of the process. We tested that the corresponding concentration of solvent solution (DMSO) did not affect the system. We let the control sample be a general control.

Then we are able to compare the DYN dataset to its corresponding control (only the solvent solution, DMSO), assuming only the disassemble rate is different between them. With these assumptions, the dynasore data helps to distinguish the correct value of each of the rates of the process. We call the disassemble rate  $k_{disC}$  for the control data, and  $k_{dis}$  for the dynasore data. We fit the control and dynasore data simultaneously to the three compartment model with  $k_{on}$ ,  $k_{off}$ ,  $k_{asm}$  and  $\delta$  same for both data sets, and  $k_{disC}$ ,  $k_{dis}$  different.

To find the confidence intervals on the parameter values, we synthetically create new sample by bootstrapping. We assume the residuals are independent and identically distributed. Bootstrap data is generated by re-sampling with replacement the residuals and add them to the best estimate solution. We consider the resulting bootstrap data as our new sample and use it to get new parameter estimates. Iterating the re-sample and fitting give us the bootstrap distribution of each parameter. This distribution is an approximation to the real distribution of the estimates and we use it to generate confidence intervals for each parameter value.

For all our datasets I refer “simple fit” to the action of solve and fit to the model (i.e. Figure 1) and then find the bootstrap distribution of the parameters; and “double fit” refers to solve and fit and find parameter confidence intervals simultaneously for the dynasore and the control datasets, with a model similar to (Figure 1) but with  $k_{disC}$  and  $k_{dis}$ , respectively.

For each of the talin mutant tested, we use our double fitting approach to find the distribution of the parameters of the control data. We select the range of the parameters from the simple fit that are closed to the double fit distribution. Remember that for each talin mutant, we analyze also the

mutant in  $\text{para}^{\text{ts2}}/\text{Brkd}^{\text{J29}}$  background. For those datasets we cannot use DYN since the permeabilization protocol by Schulman et al. (2013) only works for embryos. To overcome this, we assume that there should not be a great difference between the  $\text{para}^{\text{ts2}}/\text{Brkd}^{\text{J29}}$  data and the control data parameter estimates; at least they should be the similar order of magnitude. Therefore, we compare the parameter distributions of  $\text{para}^{\text{ts2}}/\text{Brkd}^{\text{J29}}$  datasets for each of the talin mutants with their corresponding control double fit distribution. We select the parameter distribution to be the most similar to the one of the control double fitting.

## Appendix B - Dynasore datasets used for „double fitting“.

[Experiments were performed by Pablo Lopez]

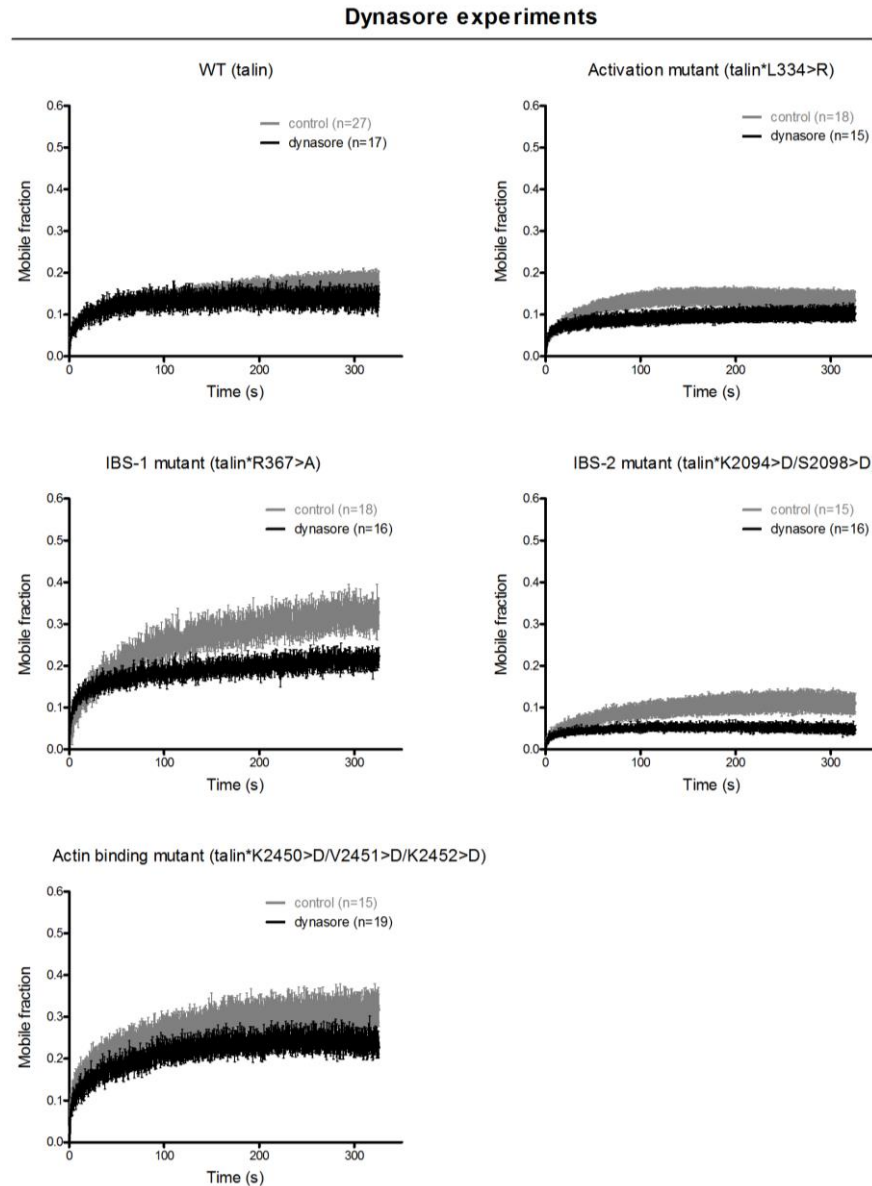


**Figure 15: Dynasore experiments used for double fitting.**

200  $\mu$ M dynasore solution was induced into embryos expressing WT talin, actin binding mutant, IBS-1 mutant and 150  $\mu$ M dynasore solution was induced into embryos expressing activation mutant and IBS-2 with protocol described in (Schulman et al., 2013) (dark curves). Control experiments performed without dynasore in the permeabilization solution (grey curves). These experiments were used for the double fitting analysis (see 2.3.2 and Figure 8 for explanation).

## Appendix C - Tables with mobile fraction and rate constant values

### C.1 WT (talin)

#### Mobile fraction

Experiment	developmental stage	temperature (°C)	Mobile Fraction	SEM	N
control	e17	25	1.52E-01	1.43E-02	15
		37	1.48E-01	9.90E-03	18
Brkd	e17	25	1.72E-01	1.78E-02	18
		37	8.66E-02	9.14E-03	22
control	L3	25	6.91E-02	4.45E-03	17
		37	5.50E-02	5.25E-03	21
para	L3	25	6.93E-02	5.22E-03	19
		37	5.88E-02	4.63E-03	21

#### Rate Constants

	Best fit			Bootstraps 95% CI		
	Parameter	Estimate	SEM	LL (2.5%)	Mean	UL (97.5%)
WT e17 25°C	kon	5.19E-03	2.60E-04	5.54E-002	6.29E-002	7.13E-002
	koff	1.30E-03	5.50E-05	4.82E-003	5.19E-003	5.59E-003
	kendo	5.16E-03	1.90E-04	1.19E-003	1.30E-003	1.40E-003
	kexo	6.27E-02	4.00E-03	4.54E-003	5.04E-003	5.50E-003
	delta	3.04E-03	4.70E-05	3.03E-003	3.13E-003	3.23E-003
	SSR = 7.180			N=2349		
WT e17 37°C	kon	1.26E-001	1.20E-002	1.03E-001	1.25E-001	1.50E-001
	koff	8.12E-003	6.30E-004	7.06E-003	8.14E-003	9.54E-003
	kendo	1.12E-003	4.20E-005	1.04E-003	1.12E-003	1.19E-003
	kexo	4.94E-003	2.70E-004	3.81E-003	4.30E-003	4.77E-003
	delta	1.48E-003	5.80E-005	1.68E-003	1.81E-003	1.94E-003
	SSR = 19.584			N=673		
BRKD 25°C	kon	4.56E-002	3.90E-003	3.87E-002	4.61E-002	5.48E-002
	koff	4.77E-003	2.10E-004	4.38E-003	4.79E-003	5.25E-003
	kendo	1.41E-003	7.50E-005	1.29E-003	1.43E-003	1.56E-003
	kexo	1.95E-003	2.70E-004	1.32E-003	1.83E-003	2.27E-003
	delta	3.05E-003	8.00E-005	3.12E-003	3.22E-003	3.32E-003
	SSR = 23.792			N=1406		
BRKD 37°C	kon	9.98E-002	1.20E-002	7.95E-002	9.99E-002	1.27E-001
	koff	5.69E-003	4.80E-004	4.86E-003	5.72E-003	6.74E-003
	kendo	8.01E-004	6.60E-005	6.77E-004	7.98E-004	9.23E-004
	kexo	7.08E-003	5.80E-004	5.60E-003	6.64E-003	7.68E-003
	delta	2.85E-003	6.30E-005	2.91E-003	3.02E-003	3.14E-003
	SSR = 32.322			N=2300		

	Best fit			Bootstraps 95% CI		
	Parameter	Estimate	SEM	LL (2.5%)	Mean	UL (97.5%)
WT L3 25°C	kon	2.08E-001	2.80E-002	1.59E-001	2.06E-001	2.67E-001
	koff	6.25E-003	6.80E-004	5.12E-003	6.27E-003	7.76E-003
	kendo	9.09E-004	4.10E-005	8.13E-004	8.88E-004	9.65E-004
	kexo	1.22E-002	4.50E-004	1.08E-002	1.16E-002	1.25E-002
	delta	1.72E-003	3.10E-005	1.76E-003	1.82E-003	1.88E-003
	SSR = 5.043			N=2575		
WT L3 37°C	kon	9.11E-002	5.90E-003	8.17E-002	9.15E-002	1.02E-001
	koff	2.87E-003	1.40E-004	2.66E-003	2.88E-003	3.15E-003
	kendo	3.38E-004	1.30E-005	3.19E-004	3.41E-004	3.64E-004
	kexo	3.38E-003	2.30E-004	2.86E-003	3.26E-003	3.67E-003
	delta	2.95E-003	2.10E-005	2.98E-003	3.05E-003	3.12E-003
	SSR = 3.514			N=1757		
PARA 25°C	kon	9.42e-02	7.1e-03	8.18E-002	9.48E-002	1.10E-001
	koff	4.70e-03	2.5e-04	4.26E-003	4.74E-003	5.28E-003
	kendo	5.65e-04	3.1e-05	5.07E-004	5.67E-004	6.29E-004
	kexo	5.50e-03	3.6e-04	4.68E-003	5.39E-003	6.08E-003
	delta	3.08e-03	3.6e-05	3.07E-003	3.15E-003	3.23E-003
	SSR = 8.146			N=1800		
PARA 37°C	kon	1.07E-001	1.00E-002	8.92E-002	1.07E-001	1.31E-001
	koff	3.48E-003	2.40E-004	3.07E-003	3.50E-003	4.05E-003
	kendo	5.19E-004	2.60E-005	4.69E-004	5.18E-004	5.71E-004
	kexo	6.38E-003	3.50E-004	5.57E-003	6.25E-003	6.92E-003
	delta	2.53E-003	2.90E-005	2.53E-003	2.58E-003	2.64E-003
	SSR = 6.818			N=1761		

## C.2 Activation mutant

### *Mobile fraction*

Experiment	developmental stage	temperature (°C)	Mobile Fraction	SEM	N
Brkd	e17	25	2.00E-01	2.23E-02	18
		37	1.61E-01	9.78E-03	24
para	L3	25	1.06E-01	1.07E-02	16
		37	9.02E-02	1.08E-02	14

### *Rate Constants*

	Best fit			Bootstraps 95% CI		
	Parameter	Estimate	SEM	LL (2.5%)	Mean	UL (97.5%)
BRKD 25°C	kon	7.80E-02	7.90E-03	6.34E-002	7.85E-002	9.67E-002
	koff	1.26E-02	9.20E-04	1.09E-002	1.27E-002	1.48E-002
	kendo	2.78E-03	1.20E-04	2.53E-003	2.79E-003	3.02E-003
	kexo	2.11E-03	2.20E-04	1.57E-003	2.07E-003	2.54E-003
	delta	7.92E-03	1.80E-04	7.72E-003	7.98E-003	8.24E-003
	SSR = 114.508			N=1540		

	Best fit			Bootstraps 95% CI		
	Parameter	Estimate	SEM	LL (2.5%)	Mean	UL (97.5%)
BRKD 37°C	kon	1.99E-03	2.20E-04	7.12E-002	7.85E-002	8.71E-002
	koff	1.14E-03	4.60E-05	9.87E-003	1.06E-002	1.15E-002
	kendo	1.06E-02	4.00E-04	1.07E-003	1.17E-003	1.26E-003
	kexo	7.82E-02	4.10E-03	1.52E-003	1.93E-003	2.35E-003
	delta	3.92E-03	7.20E-05	3.90E-003	4.04E-003	4.19E-003
	SSR = 44.990			N=1412		
PARA 25°C	kon	9.58E-02	1.10E-02	7.75E-002	9.70E-002	1.23E-001
	koff	5.44E-03	4.60E-04	4.67E-003	5.50E-003	6.55E-003
	kendo	6.89E-04	4.70E-05	6.01E-004	6.90E-004	7.82E-004
	kexo	4.30E-03	4.30E-04	3.39E-003	4.19E-003	5.01E-003
	delta	1.67E-03	6.30E-05	1.66E-003	1.72E-003	1.78E-003
	SSR = 18.27844			N=3000		
PARA 37°C	kon	1.25E-01	1.90E-02	9.20E-002	1.27E-001	1.75E-001
	koff	5.61E-03	6.80E-04	4.49E-003	5.70E-003	7.38E-003
	kendo	6.41E-04	4.40E-05	5.53E-004	6.43E-004	7.36E-004
	kexo	4.71E-03	4.60E-04	3.57E-003	4.54E-003	5.47E-003
	delta	1.83E-03	6.50E-05	1.84E-003	1.92E-003	2.00E-003
	SSR = 14.89319			N=1963		

### C.3 IBS-1 mutant

#### *Mobile fraction*

Experiment	developmental stage	temperature (°C)	Mobile Fraction	SEM	N
Brkd	e17	25	2.97E-01	2.11E-02	22
		37	1.89E-01	1.57E-02	24
para	L3	25	1.03E-01	9.21E-03	20
		37	1.05E-01	7.93E-03	21

#### *Rate Constants*

	Best fit			Bootstraps 95% CI		
	Parameter	Estimate	SEM	LL (2.5%)	Mean	UL (97.5%)
BRKD 25°C	kon	2.26E-03	2.20E-04	5.18E-002	6.10E-002	7.22E-002
	koff	3.23E-03	1.30E-04	1.09E-002	1.22E-002	1.35E-002
	kendo	1.21E-02	6.10E-04	3.00E-003	3.27E-003	3.54E-003
	kexo	6.05E-02	4.80E-03	1.73E-003	2.17E-003	2.60E-003
	delta	4.37E-03	1.50E-04	4.36E-003	4.51E-003	4.66E-003
	SSR = 144.758			N=1452		
BRKD 37°C	kon	8.59E-02	7.30E-03	7.29E-002	8.66E-002	1.03E-001
	koff	1.01E-02	6.40E-04	8.96E-003	1.02E-002	1.16E-002
	kendo	1.61E-03	6.40E-05	1.54E-003	1.66E-003	1.78E-003
	kexo	2.32E-03	2.30E-04	1.68E-003	2.11E-003	2.52E-003
	delta	3.77E-03	1.00E-04	3.98E-003	4.08E-003	4.19E-003
	SSR = 90.321			N=2694		

	Best fit			Bootstraps 95% CI		
	Parameter	Estimate	SEM	LL (2.5%)	Mean	UL (97.5%)
PARA 25°C	kon	1.14E-01	1.10E-02	9.38E-002	1.14E-001	1.38E-001
	koff	7.14E-03	5.40E-04	6.17E-003	7.16E-003	8.35E-003
	kendo	7.69E-04	3.80E-05	7.06E-004	7.79E-004	8.53E-004
	kexo	3.94E-03	3.10E-04	3.09E-003	3.68E-003	4.24E-003
	delta	2.74E-03	5.90E-05	2.86E-003	2.94E-003	3.02E-003
	SSR = 23.427			N=2988		
PARA 37°C	kon	9.94E-02	9.00E-03	8.36E-002	1.00E-001	1.20E-001
	koff	5.57E-03	3.80E-04	4.90E-003	5.60E-003	6.43E-003
	kendo	8.87E-04	3.40E-05	8.33E-004	8.96E-004	9.60E-004
	kexo	3.87E-03	2.40E-04	3.21E-003	3.66E-003	4.10E-003
	delta	3.17E-03	5.10E-05	3.26E-003	3.35E-003	3.44E-003
	SSR = 19.134			N=2981		

#### C.4 IBS-2 mutant

##### Mobile fraction

Experiment	developmental stage	temperature (°C)	Mobile Fraction	SEM	N
Brkd	e17	25	1.04E-01	1.77E-02	17
		37	6.37E-02	6.34E-03	25
para	L3	25	6.12E-02	7.69E-03	15
		37	4.09E-02	5.17E-03	13

##### Rate Constants

	Best fit			Bootstraps 95% CI		
	Parameter	Estimate	SEM	LL (2.5%)	Mean	UL (97.5%)
BRKD 25°C	kon	7.69E-02	7.80E-03	6.40E-002	7.77E-002	9.42E-002
	koff	4.37E-03	3.10E-04	3.83E-003	4.40E-003	5.02E-003
	kendo	9.67E-04	4.10E-05	9.00E-004	9.77E-004	1.05E-003
	kexo	2.87E-03	2.40E-04	2.39E-003	2.83E-003	3.26E-003
	delta	7.32E-03	6.40E-05	7.30E-003	7.44E-003	7.58E-003
	SSR=12.76			N=2231		
BRKD 37°C	kon	1.67E-01	1.90E-02	1.37E-001	1.68E-001	2.05E-001
	koff	6.63E-03	6.40E-04	5.55E-003	6.66E-003	7.94E-003
	kendo	4.03E-04	1.80E-05	3.78E-004	4.11E-004	4.44E-004
	kexo	2.19E-03	2.70E-04	1.56E-003	2.04E-003	2.53E-003
	delta	3.33E-03	4.30E-05	3.40E-003	3.52E-003	3.65E-003
	SSR=19.360			N=1898		
PARA 25°C	kon	4.75E-03	4.50E-04	7.36E-002	1.03E-001	1.47E-001
	koff	3.93E-04	2.80E-05	1.64E-003	2.14E-003	2.82E-003
	kendo	2.09E-03	2.90E-04	3.40E-004	3.93E-004	4.43E-004
	kexo	1.01E-01	1.90E-02	3.63E-003	4.47E-003	5.27E-003
	delta	1.57E-03	3.80E-05	1.62E-003	1.72E-003	1.81E-003
	SSR=6.121			N=1642		

	Best fit			Bootstraps 95% CI		
	Parameter	Estimate	SEM	LL (2.5%)	Mean	UL (97.5%)
PARA 37°C	kon	2.63E-01	5.40E-02	1.79E-001	2.63E-001	3.93E-001
	koff	5.54E-03	1.00E-03	4.00E-003	5.57E-003	8.02E-003
	kendo	3.53E-04	2.70E-05	3.01E-004	3.48E-004	3.93E-004
	kexo	8.62E-03	6.40E-04	6.89E-003	8.04E-003	9.16E-003
	delta	1.71E-03	3.30E-05	1.78E-003	1.87E-003	1.95E-003
SSR=3.495			N=2263			

## C.5 Actin binding mutant

### *Mobile fraction*

Experiment	developmental stage	temperature (°C)	Mobile Fraction	SEM	N
Brkd	e17	25	2.38E-01	3.70E-02	15
		37	1.55E-01	1.95E-02	17
para	L3	25	9.60E-02	9.01E-03	19
		37	8.34E-02	1.19E-02	17

### *Rate Constants*

	Best fit			Bootstraps 95% CI		
	Parameter	Estimate	SEM	LL (2.5%)	Mean	UL (97.5%)
BRKD 25°C	kon	5.04E-03	8.40E-04	6.32E-002	1.04E-001	1.81E-001
	koff	1.47E-03	1.60E-04	5.71E-003	8.32E-003	1.28E-002
	kendo	7.98E-03	1.50E-03	1.15E-003	1.45E-003	1.75E-003
	kexo	9.99E-02	2.50E-02	3.01E-003	4.39E-003	5.87E-003
	delta	3.30E-04	1.80E-04	3.34E-004	5.71E-004	7.62E-004
SSR = 138.867			N=1429			
BRKD 37°C	kon	4.39E-03	5.00E-04	5.31E-002	7.98E-002	1.20E-001
	koff	1.11E-03	8.70E-05	3.36E-003	4.34E-003	5.86E-003
	kendo	4.28E-03	5.70E-04	9.33E-004	1.10E-003	1.26E-003
	kexo	7.87E-02	1.60E-02	2.94E-003	3.92E-003	4.86E-003
	delta	1.48E-03	1.00E-04	1.56E-003	1.72E-003	1.88E-003
SSR = 54.382			N=1491			
PARA 25°C	kon	5.98E-03	6.10E-04	8.99E-002	1.23E-001	1.68E-001
	koff	5.81E-04	5.00E-05	4.34E-003	5.49E-003	7.10E-003
	kendo	5.45E-03	6.50E-04	4.83E-004	5.76E-004	6.71E-004
	kexo	1.23E-01	1.90E-02	4.23E-003	5.34E-003	6.45E-003
	delta	9.48E-04	6.20E-05	1.06E-003	1.16E-003	1.27E-003
SSR = 26.021			N=1629			
PARA 37°C	kon	4.98E-03	6.20E-04	9.15E-002	1.31E-001	1.88E-001
	koff	4.64E-04	4.30E-05	3.80E-003	4.99E-003	6.75E-003
	kendo	4.89E-03	6.80E-04	3.86E-004	4.65E-004	5.50E-004
	kexo	1.28E-01	2.20E-02	3.32E-003	4.48E-003	5.62E-003
	delta	9.98E-04	6.20E-05	1.11E-003	1.21E-003	1.31E-003
SSR = 20.963			N=1717			